

Ensemble Kalman Filtering-Aided Variational Inference for Gaussian Process State-Space Models

Zhidi Lin[✉], Yiyong Sun[✉], Feng Yin[✉], Senior Member, IEEE, and Alexandre Thiéry[✉]

Abstract—Gaussian process state-space models (GPSSMs) provide a principled and flexible approach to model latent state dynamics observed through emission models. However, existing variational methods for learning GPSSMs face a substantial challenge in optimizing a large number of parameters, particularly with the introduction of amortized inference networks. To address this challenge, we leverage the ensemble Kalman filter (EnKF), a well-established model-based filtering technique, to approximate the posterior distribution of latent states within the variational inference framework. This approach eliminates the need for inference networks, significantly reducing the number of variational parameters. Moreover, we demonstrate that with the aid of EnKF, the straightforward evaluation of approximated evidence lower bound (ELBO) in the variational inference can be easily obtained through the summation of multiple terms with closed-form solutions. By leveraging automatic differentiation tools, we thus can maximize the ELBO and train the GPSSM efficiently. We also extend the proposed method to an online setting and provide comprehensive algorithm analyses and insights. Extensive testing on diverse real and simulated datasets demonstrates that our variational inference algorithms, integrated with EnKF, outperform existing methods in terms of learning and inference performance.

Index Terms—Gaussian process, state-space model, ensemble Kalman filter, online learning, variational learning and inference.

I. INTRODUCTION

STATE-SPACE models (SSMs) are versatile modeling tools used to characterize dynamical patterns in time series data [1]. They have demonstrated successful applications in a wide range of fields, including engineering, statistics, computer science, and economics. The primary tasks involved in SSMs are learning and inference [2]. Learning, also known as system identification, focuses on determining optimal model parameters to accurately represent the underlying dynamical system. In contrast, inference aims to estimate latent states of interest based on observed sequential data [1]–[3].

Over the past few decades, numerous learning and inference methods have been developed for SSMs. In cases where the system dynamics are precisely known, various well-established techniques such as the Kalman filter (KF), extended Kalman filter (EKF), ensemble Kalman filter (EnKF) and particle filter (PF) can be employed to infer the latent states [1]. However, in

Z. Lin is with the Future Network of Intelligence Institute, and the School of Science & Engineering, The Chinese University of Hong Kong (Shenzhen), Shenzhen 518172, China, and also with the Shenzhen Research Institute of Big Data, Shenzhen 518172, China (email: zhidi.lin@link.cuhk.edu.cn)

Y. Sun and F. Yin are with the School of Science & Engineering, The Chinese University of Hong Kong (Shenzhen), Shenzhen 518172, China (email: yiyong.sun@link.cuhk.edu.cn, yinfeng@cuhk.edu.cn). F. Yin is the corresponding author.

A. Thiéry is with the Department of Statistics & Data Science, National University of Singapore, Singapore 117546 (email: a.h.thiery@nus.edu.sg).

complex and uncertain scenarios like model-based reinforcement learning [4], [5] and disease epidemic propagation [6], knowing and determining the underlying system dynamics in advance poses tremendous challenges [7]. Thus, the dynamics need to be learned from the observed noisy measurements, leading to the emergence of data-driven state-space models. One class of prominent data-driven state-space models is the Gaussian process state-space model (GPSSM) [8], which utilizes Gaussian processes (GPs) as core components to capture the complex dynamics of the underlying system [9].

The popularity of GPSSM is largely driven by its inherent appealing properties [8]. First, GPSSM is a probabilistic SSM, offering interpretability and explicit uncertainty calibration for the system dynamics [10]. Second, the nonparametric GP models in GPSSM enable automatic adaptation to problem complexity. Consequently, in practice, GPSSMs often achieve high accuracy in model learning even with limited data [2].

Despite the numerous advantageous properties of GPSSMs, the task of learning and inference in GPSSMs remains challenging. Early studies primarily focused on the following two approaches: (1) inferring the latent states through *maximum a posteriori* (MAP) estimation [10]–[13], and/or (2) learning GPSSM transition function by assuming the observable latent states [14]–[16]. However, the MAP estimation is limited to providing a point estimate and often fails to accurately capture the mode of the posterior distribution [3], while assuming observable latent states for learning transition function is often impractical in various applications [17]. These challenges have led to a limited applicability of the earlier GPSSM works.

To overcome these challenges, the seminal work in [18] introduces a fully Bayesian framework, utilizing Monte Carlo sampling techniques for simultaneous learning and inference of the GPSSM. Subsequently, more advanced approximation methods [19]–[21] leverage the GP approximation from [22] to alleviate the substantial computational demands in [18]. However, the computational burden associated with Monte Carlo sampling methods, particularly when dealing with high-dimensional latent states, remains notably significant. Consequently, there has been a shift towards variational inference methods [23]–[29] that combine with the utilization of sparse GPs featuring inducing points [30]. Typically, the variational inference approaches can be classified into two categories: the mean-field (MF) class [8], [23]–[25], and the non-mean-field (NMF) class [26]–[29], based on whether the independence assumption is applied to the variational distribution concerning the GP-based transition function and latent state.

The first MF variational algorithm that incorporates a PF for latent state inference is introduced in [23]. To address the computational complexity inherent in the PF, the work in

[24] proposes the utilization of a (parametric) linear Markov Gaussian variational distribution for the latent states. However, this approach presents an issue of linear growth in the number of variational parameters over time. In response, the authors in [25] present a solution by leveraging an amortized inference network [31] to model the variational distribution effectively. In subsequent research endeavors, the focus has shifted towards the NMF algorithm, aiming to improve inference accuracy and mitigate issues of over-confidence [32].

The first NMF variational algorithm is proposed in [26], where the posterior distribution of the latent states conditioning on the GP transition function is directly approximated using the prior distribution. However, this approximation lacks the incorporation of observation information in the posterior, rendering filtering or smoothing infeasible. To address this issue, the work in [27] explicitly assumes a flexible parametric Markov-structured Gaussian variational distribution over the latent states, and propose an algorithm called VCDT (variationally coupled dynamics and trajectories). In [28], the authors propose a forward-backward smoothing-like variational learning method to address learning in unstable systems with partial observability. In [29], the Laplace approximation is employed to approximate the posterior distribution, resulting in a linear Markov Gaussian approximation similar to [25]. Other recent works have highlighted the advantageous impact of increased GPSSM's flexibility on learning and inference performance [33]–[37].

Nevertheless, the existing methods suffer from two significant limitations. First, the state-of-the-art NMF assumption on the variational distribution could still be oversimplified, which may overlook the intricacies of the underlying dynamics [38]. Second, optimizing the amortized inference network in state-of-the-art methods [25]–[28], [36] presents notable computational challenges due to the substantial data requirements and the inherent risk of encountering numerous bad local optima during the optimization process [2]. In response to the first limitation, a very recent work [38] proposes using a free-form variational distribution in combination with stochastic gradient Hamiltonian Monte Carlo [39]. In this paper, we focus on the second limitation. Specifically, our objective is to alleviate the optimization and computational burden by eliminating the need for additional variational parameters and black-box inference networks. The main contributions of this paper are summarized as follows.

- We highlight the significance of incorporating well-established model-based filtering techniques in developing GPSSM variational algorithms. In contrast to existing methods relying on inference networks with numerous variational parameters for learning variational distribution, we introduce a novel EnKF-aided NMF variational inference algorithm tailored for GPSSMs. This novel approach eliminates the need for an inference network, resulting in a substantial reduction in variational parameters, thereby enhancing learning efficiency.
- In addition, with the aid of EnKF, we demonstrate that the straightforward evaluation of approximated evidence lower bound (ELBO) in the variational inference can be easily obtained by summing multiple terms with

closed-form analytical solutions. By harnessing automatic differentiation tools, we thus can efficiently optimize the ELBO and train the GPSSM.

- Without the burden of inference network, the proposed EnKF-aided algorithm gets readily extended to an online learning setting. This online extension introduces a more comprehensive objective function, making it superior to state-of-the-art online algorithms in learning and inference efficiency.
- We provide comprehensive analysis and profound insights into the proposed algorithms and conduct extensive experiments on various real and synthetic datasets to evaluate the algorithms' performance. The results demonstrate that the proposed EnKF-aided variational learning methods consistently outperform existing state-of-the-art methods in terms of learning and inference performance.

The remainder of this paper is organized as follows. Some preliminaries related to GPSSMs are provided in Section II. The problems addressed in this paper are summarized in Section III. Section IV elaborates the proposed EnKF-aided variational learning algorithm. Section V extends the proposed algorithm to the online setting. The experimental results are presented in Section VI, and Section VII concludes this paper. More supportive results, proofs, etc. are relegated to the Appendix and supplementary materials.

II. PRELIMINARIES

In Section II-A, we briefly review the Gaussian process regression. Section II-B is dedicated to introducing Gaussian process state-space models.

A. Gaussian Processes (GPs)

A GP defines a collection of random variables indexed by $\mathbf{x} \in \mathcal{X}$, such that any finite subset of these variables follows a joint Gaussian distribution [9]. Mathematically, a real scalar-valued GP $f(\mathbf{x})$ can be written as

$$f(\mathbf{x}) \sim \mathcal{GP}(\mu(\mathbf{x}), k(\mathbf{x}, \mathbf{x}'); \theta_{gp}), \quad (1)$$

where $\mu(\mathbf{x})$ is a mean function typically set to zero in practice, and $k(\mathbf{x}, \mathbf{x}')$ is the covariance function, also known as kernel function, which is interpretable and can provide insights about the nature of the underlying function [9]; and θ_{gp} is a set of hyperparameters that needs to be tuned for model selection.

Let us consider a general regression model,

$$y = f(\mathbf{x}) + e, \quad e \sim \mathcal{N}(0, \sigma_e^2), \quad y \in \mathbb{R}. \quad (2)$$

By placing a GP prior over the function $f(\cdot) : \mathcal{X} \mapsto \mathbb{R}$, we get the salient Gaussian process regression (GPR) model. The task in GPR model is to infer the mapping function $f(\cdot)$ using an observed dataset $\mathcal{D} \triangleq \{\mathbf{x}_i, y_i\}_{i=1}^n \triangleq \{\mathbf{X}, \mathbf{y}\}$ consisting of n samples, or alternatively input-output pairs. Conditioning on the observed data, the posterior distribution of the mapping function, $p(f(\mathbf{x}_*) | \mathbf{x}_*, \mathcal{D})$, at any test input $\mathbf{x}_* \in \mathcal{X}$, is Gaussian, fully characterized by the posterior mean ξ and the posterior variance Ξ . Concretely,

$$\xi(\mathbf{x}_*) = \mathbf{K}_{\mathbf{x}_*, \mathbf{X}} (\mathbf{K}_{\mathbf{X}, \mathbf{X}} + \sigma_e^2 \mathbf{I}_n)^{-1} \mathbf{y}, \quad (3a)$$

$$\Xi(\mathbf{x}_*) = \mathbf{K}_{\mathbf{x}_*, \mathbf{X}} (\mathbf{K}_{\mathbf{X}, \mathbf{X}} + \sigma_e^2 \mathbf{I}_n)^{-1} \mathbf{K}_{\mathbf{x}_*, \mathbf{X}}^\top, \quad (3b)$$

where $\mathbf{K}_{\mathbf{X}, \mathbf{X}}$ denotes the covariance matrix evaluated on the training input \mathbf{X} , and each entry is $[\mathbf{K}_{\mathbf{X}, \mathbf{X}}]_{i,j} = k(\mathbf{x}_i, \mathbf{x}_j)$; $\mathbf{K}_{\mathbf{x}_*, \mathbf{X}}$ denotes the cross covariance matrix between the test input \mathbf{x}_* and the training input \mathbf{X} ; the zero-mean GP prior is assumed here and will be used in the rest of this paper if there is no further specification. Note that the posterior distribution $p(f(\mathbf{x}_*)|\mathbf{x}_*, \mathcal{D})$ gives not only a point estimate, i.e., the posterior mean, but also an uncertainty region of such estimate quantified by the posterior variance. It should also be noted that here we denote the variables in the GPR model using mathematical mode italics, such as \mathbf{x}_i and \mathbf{y}_i ; these variables should not be confused with the latent state \mathbf{x}_t and observation \mathbf{y}_t in SSM (cf. Eq. (4)).

B. Gaussian Process State-Space Models (GPSSMs)

A generic SSM describes the probabilistic dependence between latent state $\mathbf{x}_t \in \mathbb{R}^{d_x}$ and observation $\mathbf{y}_t \in \mathbb{R}^{d_y}$. Mathematically, it can be expressed by the following equations:

$$(Transition) \quad \mathbf{x}_{t+1} = f(\mathbf{x}_t) + \mathbf{v}_t, \quad \mathbf{v}_t \sim \mathcal{N}(\mathbf{0}, \mathbf{Q}), \quad (4a)$$

$$(Emission) \quad \mathbf{y}_t = \mathbf{C}\mathbf{x}_t + \mathbf{e}_t, \quad \mathbf{e}_t \sim \mathcal{N}(\mathbf{0}, \mathbf{R}), \quad (4b)$$

where the latent states form a Markov chain. That is, for any time instance $t \in \mathbb{N}$, the next state \mathbf{x}_{t+1} is generated by conditioning on only \mathbf{x}_t and the transition function $f(\cdot) : \mathbb{R}^{d_x} \mapsto \mathbb{R}^{d_x}$. The emission is assumed to be linear with a known coefficient matrix, $\mathbf{C} \in \mathbb{R}^{d_y \times d_x}$, hence mitigating the system non-identifiability¹. The initial state distribution $p(\mathbf{x}_0)$ is also known and assumed to follow a Gaussian distribution. Both the states and observations are corrupted by zero-mean Gaussian noise with covariance matrices \mathbf{Q} and \mathbf{R} , respectively.

The GPSSM incorporates a GP prior to model the transition function $f(\cdot)$ in Eq. (4). Specifically, Fig. 1 presents the graphical model of GPSSM, while the following equations express its formulation:

$$f(\cdot) \sim \mathcal{GP}(\mu(\cdot), k(\cdot, \cdot); \theta_{gp}) \quad (5a)$$

$$\mathbf{x}_0 \sim p(\mathbf{x}_0) \quad (5b)$$

$$\mathbf{f}_t = f(\mathbf{x}_{t-1}) \quad (5c)$$

$$\mathbf{x}_t \mid \mathbf{f}_t \sim \mathcal{N}(\mathbf{x}_t \mid \mathbf{f}_t, \mathbf{Q}) \quad (5d)$$

$$\mathbf{y}_t \mid \mathbf{x}_t \sim \mathcal{N}(\mathbf{y}_t \mid \mathbf{C}\mathbf{x}_t, \mathbf{R}) \quad (5e)$$

where \mathbf{f}_t represents the GP transition function value evaluated at the previous state \mathbf{x}_{t-1} . Note that when dealing with a multidimensional state space ($d_x > 1$), the transition function $f(\cdot) : \mathbb{R}^{d_x} \mapsto \mathbb{R}^{d_x}$ is represented using a multi-output GP. In this context, the d_x functions are typically modeled with d_x mutually independent GPs [35]. Furthermore, it is worth noting that the GPSSM illustrated in Fig. 1 can be extended to accommodate control systems incorporating a deterministic control input $\mathbf{c}_t \in \mathbb{R}^{d_c}$ by augmenting the latent state with $[\mathbf{x}_t, \mathbf{c}_t] \in \mathbb{R}^{d_x+d_c}$. For the sake of brevity, however, we omit explicit reference to \mathbf{c}_t in our notation throughout this paper.

¹Nonlinear emissions can be addressed by augmenting the latent state to a higher dimension. This augmentation helps mitigate/eliminate the significant non-identifiability issues commonly encountered in GPSSMs [8], [36]

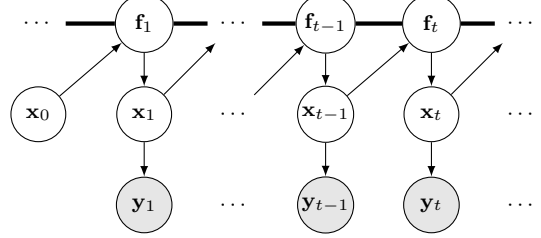


Fig. 1. Graphical model of GPSSM. The white circles represent the latent variables, while the gray circles represent the observable variables. The thick horizontal bar represents a set of fully connected nodes, i.e., the GP.

Given the aforementioned model descriptions, the joint density function of the GPSSM can be expressed as:

$$p(\vec{\mathbf{f}}, \vec{\mathbf{x}}, \vec{\mathbf{y}} | \boldsymbol{\theta}) = p(\mathbf{x}_0)p(\mathbf{f}_{1:T}) \prod_{t=1}^T p(\mathbf{y}_t | \mathbf{x}_t)p(\mathbf{x}_t | \mathbf{f}_t), \quad (6)$$

where $p(\mathbf{f}_{1:T}) = p(f(\mathbf{x}_{0:T-1})) = \prod_{t=1}^T p(\mathbf{f}_t | \mathbf{f}_{1:t-1}, \mathbf{x}_{0:t-1})$ corresponds to a finite dimensional (T -dimensional) GP distribution [8], and we define the short-hand notations $\vec{\mathbf{y}} \triangleq \mathbf{y}_{1:T} = \{\mathbf{y}_t\}_{t=1}^T$, $\vec{\mathbf{f}} \triangleq \mathbf{f}_{1:T} = \{\mathbf{f}_t\}_{t=1}^T$, and $\vec{\mathbf{x}} \triangleq \mathbf{x}_{0:T} = \{\mathbf{x}_t\}_{t=0}^T$. The model parameters $\boldsymbol{\theta}$ includes the noise covariance and GP hyper-parameters, i.e., $\boldsymbol{\theta} = [\mathbf{Q}, \mathbf{R}, \theta_{gp}]$. The challenging task in GPSSM is to learn $\boldsymbol{\theta}$, and simultaneously infer the latent states of interest, which usually involves the marginal distribution $p(\vec{\mathbf{y}} | \boldsymbol{\theta})$. However, due to the nonlinearity of GP, a closed-form analytical solution for $p(\vec{\mathbf{y}} | \boldsymbol{\theta})$ is unavailable. Hence, it becomes necessary to utilize approximation methods.

III. PROBLEM STATEMENT

To overcome the intractability of the marginal distribution $p(\vec{\mathbf{y}} | \boldsymbol{\theta})$, variational GPSSMs involve constructing an ELBO, denoted by \mathcal{L} , to the logarithm of the marginal likelihood, $\log p(\vec{\mathbf{y}} | \boldsymbol{\theta})$. Specifically, the ELBO is constructed such that the difference between $\log p(\vec{\mathbf{y}} | \boldsymbol{\theta})$ and \mathcal{L} is equal to the Kullback-Leibler (KL) divergence between the variational approximation, $q(\vec{\mathbf{x}}, \vec{\mathbf{f}})$, and the true posterior, $p(\vec{\mathbf{x}}, \vec{\mathbf{f}} | \vec{\mathbf{y}})$, i.e.,

$$\log p(\vec{\mathbf{y}} | \boldsymbol{\theta}) - \underbrace{\mathbb{E}_{q(\vec{\mathbf{x}}, \vec{\mathbf{f}})} \left[\log \frac{p(\vec{\mathbf{f}}, \vec{\mathbf{x}}, \vec{\mathbf{y}})}{q(\vec{\mathbf{x}}, \vec{\mathbf{f}})} \right]}_{\triangleq \mathcal{L}} = \underbrace{\text{KL}[q(\vec{\mathbf{x}}, \vec{\mathbf{f}}) \| p(\vec{\mathbf{x}}, \vec{\mathbf{f}} | \vec{\mathbf{y}})]}_{\geq 0} \quad (7)$$

See detailed derivations in Supplement A-A. Maximizing \mathcal{L} w.r.t. $\boldsymbol{\theta}$ fine-tunes the model parameters to improve the fit with the observed data, reflecting the model learning process; while maximizing \mathcal{L} w.r.t. the variational distribution $q(\vec{\mathbf{x}}, \vec{\mathbf{f}})$ is equivalent to minimizing the KL divergence, $\text{KL}[q(\vec{\mathbf{x}}, \vec{\mathbf{f}}) \| p(\vec{\mathbf{x}}, \vec{\mathbf{f}} | \vec{\mathbf{y}})]$. That is, it enhances the quality of the variational distribution approximation, bringing it closer to the underlying posterior distribution, $p(\vec{\mathbf{x}}, \vec{\mathbf{f}} | \vec{\mathbf{y}})$, which corresponds to the model inference process [40]. The capacity of $q(\vec{\mathbf{x}}, \vec{\mathbf{f}})$ to approximate $p(\vec{\mathbf{x}}, \vec{\mathbf{f}} | \vec{\mathbf{y}})$ is thus of crucial importance [41].

Based on the model defined in Eq. (6), a generic factorization of $q(\vec{\mathbf{x}}, \vec{\mathbf{f}})$ is as follows:

$$q(\vec{\mathbf{x}}, \vec{\mathbf{f}}) = q(\mathbf{x}_0)q(\vec{\mathbf{f}}) \prod_{t=1}^T q(\mathbf{x}_t | \mathbf{f}_t), \quad (8)$$

where $q(\vec{\mathbf{f}})$ represents the variational distribution of the GP and $q(\mathbf{x}_0) \prod_{t=1}^T q(\mathbf{x}_t | \mathbf{f}_t)$ corresponds to the variational distribution of the latent states [36], [42]. It is noteworthy that the factorization of the variational distribution presented in Eq. (8) is recognized as a NMF approximation within the GPSSM literature (see formal definition in Appendix C) [27], because it explicitly establishes the dependence between the latent states and the GP transition function values, as manifested by the terms $\prod_{t=1}^T q(\mathbf{x}_t | \mathbf{f}_t)$.

The first notable NMF approximation approach is proposed by Doerr *et al.* in [26], where $q(\mathbf{x}_t | \mathbf{f}_t)$ is set equal to the prior distribution $p(\mathbf{x}_t | \mathbf{f}_t)$, i.e., $q(\mathbf{x}_t | \mathbf{f}_t) = p(\mathbf{x}_t | \mathbf{f}_t)$. Although there is a dependence between latent states $\vec{\mathbf{x}}$ and transition function values $\vec{\mathbf{f}}$, there is no filtering or smoothing effect for latent states [27]. Instead, Ialongo *et al.* assume a flexible, parametric Markov-structured Gaussian variational distribution over the temporal states, i.e.,

$$q(\mathbf{x}_t | \mathbf{f}_t) = \mathcal{N}(\mathbf{x}_t | \mathbf{A}_t \mathbf{f}_t + \mathbf{b}_t, \mathbf{S}_t), \quad (9)$$

where $\{\mathbf{A}_t, \mathbf{b}_t, \mathbf{S}_t\}_{t=1}^T$ are free variational parameters. This choice, however, introduces a significant drawback: the number of variational parameters grows linearly with the length of the time series. Although this issue can be partially addressed by incorporating an *inference network*, such as a bidirectional recurrent neural network (Bi-RNN) [25], [42], to amortize the inference process, fine-tuning the large variational parameters in the inference network still requires substantial effort. Consequently, despite the flexibility of the variational distribution described in Eq. (9) allowing for approximation of the true posterior distribution, its empirical performance often falls short of its theoretical expressive capacity [29]. Moreover, it is worth noting that the inference network commonly takes the input of the observations, $\vec{\mathbf{y}}$, rendering the existing inference network-based methods predominantly trained in an offline manner, thus posing challenges when attempting to adapt them for online applications. To address these limitations, this paper proposes a novel approach that combines well-established EnKF with modern automatic differentiation tools [43] for variational inference in GPSSMs. The objective is to alleviate the optimization and computational burden, as well as to develop a more interpretable approach, stepping away from black-box inference networks.

IV. ENVI: ENKF-AIDED VARIATIONAL INFERENCE

This section presents our novel variational inference algorithm for GPSSMs. We begin by introducing the model-based EnKF in Section IV-A, which serves as the foundation for our algorithm. Following that, Section IV-B details the proposed EnKF-aided variational inference algorithm. Lastly, extensive discussions about the properties of our proposed method are given in Section IV-C.

A. Ensemble Kalman Filter (EnKF)

Given a SSM, see Eq. (4), the EnKF sequentially approximates the filtering distributions using $N \in \mathbb{N}$ equally weighted particles [44]. Specifically, at the prediction step, EnKF first samples particles, $\mathbf{x}_{t-1}^{1:N} \triangleq \{\mathbf{x}_{t-1}^n\}_{n=1}^N$, from the filtering

distribution at time $t-1$, $p(\mathbf{x}_{t-1} | \mathbf{y}_{1:t-1})$. Then, the sampled particles are propagated using the state transition function $f(\cdot)$, i.e.,

$$\bar{\mathbf{x}}_t^n = f(\mathbf{x}_{t-1}^n) + \mathbf{v}_t^n, \quad \mathbf{v}_t^n \sim \mathcal{N}(0, \mathbf{Q}), \quad \forall n. \quad (10)$$

The prediction distribution is then approximated by a Gaussian distribution, i.e. $p(\mathbf{x}_t | \mathbf{y}_{1:t-1}) \approx \mathcal{N}(\bar{\mathbf{x}}_t | \bar{\mathbf{m}}_t, \bar{\mathbf{P}}_t)$, where

$$\bar{\mathbf{m}}_t = \frac{1}{N} \sum_{n=1}^N \bar{\mathbf{x}}_t^n, \quad (11a)$$

$$\bar{\mathbf{P}}_t = \frac{1}{N-1} \sum_{n=1}^N (\bar{\mathbf{x}}_t^n - \bar{\mathbf{m}}_t)(\bar{\mathbf{x}}_t^n - \bar{\mathbf{m}}_t)^\top. \quad (11b)$$

With the linear Gaussian emission in Eq. (4), the joint distribution of \mathbf{x}_t and \mathbf{y}_t can be expressed as follows:

$$\begin{bmatrix} \mathbf{x}_t | \mathbf{y}_{1:t-1} \\ \mathbf{y}_t | \mathbf{y}_{1:t-1} \end{bmatrix} \sim \mathcal{N} \left(\begin{bmatrix} \bar{\mathbf{m}}_t \\ C\bar{\mathbf{m}}_t \end{bmatrix}, \begin{bmatrix} \bar{\mathbf{P}}_t, & \bar{\mathbf{P}}_t \mathbf{C}^\top \\ C\bar{\mathbf{P}}_t, & C\bar{\mathbf{P}}_t \mathbf{C}^\top + \mathbf{R} \end{bmatrix} \right). \quad (12)$$

Thus, at the update step, the filtering distribution, $p(\mathbf{x}_t | \mathbf{y}_{1:t}) = \mathcal{N}(\mathbf{x}_t | \mathbf{m}_t, \mathbf{P}_t)$, can be obtained using conditional Gaussian identity, where

$$\mathbf{m}_t = \bar{\mathbf{m}}_t + \bar{\mathbf{G}}_t(\mathbf{y}_t - C\bar{\mathbf{m}}_t), \quad (13a)$$

$$\mathbf{P}_t = \bar{\mathbf{P}}_t - \bar{\mathbf{P}}_t \mathbf{C}^\top \bar{\mathbf{G}}_t^\top, \quad (13b)$$

and $\bar{\mathbf{G}}_t = \bar{\mathbf{P}}_t \mathbf{C}^\top (C\bar{\mathbf{P}}_t \mathbf{C}^\top + \mathbf{R})^{-1}$ is the Kalman gain [44]. Each filtered particle \mathbf{x}_t^n is then obtained from a Kalman-type update, i.e.,

$$\mathbf{x}_t^n = \bar{\mathbf{x}}_t^n + \bar{\mathbf{G}}_t(\mathbf{y}_t + \mathbf{e}_t^n - C\bar{\mathbf{x}}_t^n), \quad \mathbf{e}_t^n \sim \mathcal{N}(0, \mathbf{R}), \quad \forall n. \quad (14)$$

In the following subsections, we will describe our novel integration of the variational inference framework with the EnKF [44], which leads to a reduction in variational parameters and ultimately enhances the learning and inference performance of GPSSMs.

B. EnKF-Aided Variational Inference (EnVI)

1) **Sparse GPSSMs:** Before introducing the utilization of EnKF, we first introduce the sparse GP [30], [45], a widely utilized technique in various GP variational approximations. This method serves as a scalable approach to model the corresponding GP component within the approximate posterior distribution (see Eq. (8)), thereby guaranteeing inherent scalability in GPSSM. The main idea of the sparse GPs is to introduce a small set of inducing points $\vec{\mathbf{z}} \triangleq \{\mathbf{z}_i\}_{i=1}^M$ and $\vec{\mathbf{u}} \triangleq \{\mathbf{u}_i\}_{i=1}^M$, $M \ll T$, to serve as the surrogate of the associated GPs, where the inducing inputs, $\mathbf{z}_i \in \mathbb{R}^{d_x}$, $\forall i$, are placed in the same space as the latent states \mathbf{x}_t , while the corresponding inducing outputs $\mathbf{u}_i = f(\mathbf{z}_i)$ follow the same GP prior as $\vec{\mathbf{f}}$. With the augmentation of the inducing points, the joint distribution of the GPSSM becomes

$$p(\vec{\mathbf{f}}, \vec{\mathbf{u}}, \vec{\mathbf{x}}, \vec{\mathbf{y}}) = p(\mathbf{x}_0) p(\vec{\mathbf{f}}, \vec{\mathbf{u}}) \prod_{t=1}^T p(\mathbf{y}_t | \mathbf{x}_t) p(\mathbf{x}_t | \mathbf{f}_t), \quad (15)$$

where $p(\vec{\mathbf{f}}, \vec{\mathbf{u}}) = p(\vec{\mathbf{u}}) p(\vec{\mathbf{f}} | \vec{\mathbf{u}}) = p(\vec{\mathbf{u}}) \prod_{t=1}^T p(\mathbf{f}_t | \mathbf{x}_{t-1}, \vec{\mathbf{u}})$ is the augmented GP prior and $p(\mathbf{f}_t | \mathbf{x}_{t-1}, \vec{\mathbf{u}})$ is the noiseless GP prediction whose mean and covariance can be computed

similarly to Eq. (3). The introduced inducing inputs \vec{z} will be treated as variational parameters and jointly optimized with model parameters [45]. We will further describe this later.

Suppose that the inducing outputs \vec{u} serve as sufficient statistics for the GP function values \vec{f} , such that given \vec{u} , the GP function values \vec{f} and any novel \mathbf{f}_* are independent [30], i.e., $p(\mathbf{f}_*|\vec{f}, \vec{u}) = p(\mathbf{f}_*|\vec{u})$ for any \mathbf{f}_* . We can integrate out \vec{f} in Eq. (15), and the transition function is fully characterized using only the inducing points. Consequently, we have:

$$p(\vec{u}, \vec{x}, \vec{y}) = p(\mathbf{x}_0)p(\vec{u}) \prod_{t=1}^T p(\mathbf{y}_t|\mathbf{x}_t)p(\mathbf{x}_t|\vec{u}, \mathbf{x}_{t-1}), \quad (16)$$

where

$$\begin{aligned} p(\mathbf{x}_t|\vec{u}, \mathbf{x}_{t-1}) &= \int p(\mathbf{x}_t|\mathbf{f}_t)p(\mathbf{f}_t|\mathbf{x}_{t-1}, \vec{u}, \vec{z})d\mathbf{f}_t \\ &= \mathcal{N}(\mathbf{x}_t \mid \boldsymbol{\xi}_t, \boldsymbol{\Xi}_t), \end{aligned} \quad (17)$$

and with a bit abuse of notation,

$$\boldsymbol{\xi}_t = \mathbf{K}_{\mathbf{x}_{t-1}, \vec{z}}(\mathbf{K}_{\vec{z}, \vec{z}} + \mathbf{Q})^{-1}\vec{u}, \quad (18a)$$

$$\boldsymbol{\Xi}_t = \mathbf{K}_{\mathbf{x}_{t-1}, \mathbf{x}_{t-1}} + \mathbf{Q} - \mathbf{K}_{\mathbf{x}_{t-1}, \vec{z}}(\mathbf{K}_{\vec{z}, \vec{z}} + \mathbf{Q})^{-1}\mathbf{K}_{\mathbf{x}_{t-1}, \vec{z}}. \quad (18b)$$

That is to say, with the aid of sparse GPs, the computational complexity of GPSSMs can be reduced to $\mathcal{O}(d_x T M^2)$, comparing to the original $\mathcal{O}(d_x T^3)$ [36].

2) **ELBO for sparse GPSSM:** In the context of the GPSSM described in Eq. (16), we first assume a generic variational distribution for the latent variables, $\{\vec{u}, \vec{x}\}$, factorized as follows:

$$\begin{aligned} q(\vec{u}, \vec{x}) &= q(\vec{u})q(\mathbf{x}_0) \prod_{t=1}^T \int q(\mathbf{x}_t|\mathbf{f}_t)p(\mathbf{f}_t|\vec{u}, \mathbf{x}_{t-1})d\mathbf{f}_t \\ &= q(\vec{u})q(\mathbf{x}_0) \prod_{t=1}^T q(\mathbf{x}_t|\vec{u}, \mathbf{x}_{t-1}). \end{aligned} \quad (19)$$

Here, the variational distribution over the inducing outputs, $q(\vec{u})$, is explicitly assumed to be a free-form Gaussian, i.e.,

$$q(\vec{u}) = \prod_{d=1}^{d_x} \mathcal{N}(\{\mathbf{u}_{i,d}\}_{i=1}^M \mid \mathbf{m}_d, \mathbf{L}_d \mathbf{L}_d^\top) = \mathcal{N}(\vec{u} \mid \mathbf{m}, \mathbf{S}), \quad (20)$$

where $\mathbf{m} = [\mathbf{m}_1^\top, \dots, \mathbf{m}_{d_x}^\top]^\top \in \mathbb{R}^{M d_x}$ and $\mathbf{S} = \text{diag}(\mathbf{L}_1 \mathbf{L}_1^\top, \dots, \mathbf{L}_{d_x} \mathbf{L}_{d_x}^\top) \in \mathbb{R}^{M d_x \times M d_x}$ are free variational parameters. This explicit representation of the variational distribution enables scalability through the utilization of stochastic gradient-based optimization [46], as it allows for the independence of individual GP predictions given the explicit inducing points [45]. Similarly, we assume that the variational distribution over the initial state is $q(\mathbf{x}_0) = \mathcal{N}(\mathbf{x}_0 \mid \mathbf{m}_0, \mathbf{L}_0 \mathbf{L}_0^\top)$, where $\mathbf{m}_0 \in \mathbb{R}^{d_x}$ and lower-triangular matrix $\mathbf{L}_0 \in \mathbb{R}^{d_x \times d_x}$ are free variational parameters of $q(\mathbf{x}_0)$. The variational distribution of the latent states, $q(\mathbf{x}_t|\vec{u}, \mathbf{x}_{t-1})$, obtained by integrating out \mathbf{f}_t as shown in Eq. (19), will be modeled by resorting to the EnKF technique. This modeling approach will help eliminate the need for the parameterized variational distribution, a common requirement in the existing works [25]–[28], thus overcoming the challenges associated with optimizing a large number of parameters in black-box inference networks, as discussed in Section III.

Before elucidating the methodology of employing EnKF to eliminate the parameterized assumptions associated with $q(\mathbf{x}_t|\vec{u}, \mathbf{x}_{t-1})$, let us first undertake the derivation of the ELBO induced by Eq. (16) and Eq. (19). After performing certain algebraic calculations, the ELBO is obtained as

$$\begin{aligned} \mathcal{L} &= \mathbb{E}_{q(\vec{u}, \vec{x})} \left[\log \frac{p(\vec{u}, \vec{x}, \vec{y})}{q(\vec{u}, \vec{x})} \right] \\ &= \mathbb{E}_{q(\vec{u}, \vec{x})} \left[\log \frac{p(\mathbf{x}_0)p(\vec{u}) \prod_{t=1}^T p(\mathbf{x}_t|\vec{u}, \mathbf{x}_{t-1})p(\mathbf{y}_t|\mathbf{x}_t)}{q(\vec{u})q(\mathbf{x}_0) \prod_{t=1}^T q(\mathbf{x}_t|\vec{u}, \mathbf{x}_{t-1})} \right] \\ &= \underbrace{\mathbb{E}_{q(\vec{u}, \vec{x})} \left[\sum_{t=1}^T \log p(\mathbf{y}_t|\mathbf{x}_t) \right]}_{\text{term 1}} - \underbrace{\text{KL}[q(\mathbf{x}_0) \parallel p(\mathbf{x}_0)]}_{\text{term 2}} \\ &\quad - \underbrace{\text{KL}[q(\vec{u}) \parallel p(\vec{u})]}_{\text{term 3}} - \underbrace{\mathbb{E}_{q(\vec{u}, \vec{x})} \left[\sum_{t=1}^T \log \frac{q(\mathbf{x}_t|\vec{u}, \mathbf{x}_{t-1})}{p(\mathbf{x}_t|\vec{u}, \mathbf{x}_{t-1})} \right]}_{\text{term 4}}. \end{aligned} \quad (21)$$

Remark 1. Each component of the ELBO in Eq. (21) is interpretable. More specifically,

- Term 1 corresponds to the data reconstruction error, which encourages any state trajectory \vec{x} sampled from the variational distribution, $q(\vec{u}, \vec{x})$, to accurately reconstruct the observed data.
- Terms 2 and 3 serve as regularization terms for $q(\mathbf{x}_0)$ and $q(\vec{u})$, respectively. They discourage significant deviations of the variational distributions from the corresponding prior distributions.
- Term 4 represents a regularization for $q(\mathbf{x}_t|\vec{u}, \mathbf{x}_{t-1})$, which discourages significant deviations of $q(\mathbf{x}_t|\vec{u}, \mathbf{x}_{t-1})$ from the prior $p(\mathbf{x}_t|\vec{u}, \mathbf{x}_{t-1})$.

3) **EnVI algorithm:** We next proceed to outline the approximate evaluation of the ELBO in Eq. (21) using EnKF. The main idea involves employing the filtering distribution obtained from EnKF as a substitute for the corresponding variational distribution, serving as an approximation for the true posterior distribution, $p(\mathbf{x}_t|\vec{u}, \vec{y})$.

Building upon the EnKF outlined in Section IV-A and assuming that at time step $t-1$, we have acquired the variational distribution, $q(\mathbf{x}_{t-1}|\vec{u}) \triangleq p(\mathbf{x}_{t-1}|\vec{u}, \mathbf{y}_{1:t-1}) = \mathcal{N}(\mathbf{x}_{t-1} \mid \mathbf{m}_{t-1}, \mathbf{P}_{t-1})$, we employ the GP transition, presented in Eq. (17), to perform the prediction step and generate N predicted samples $\bar{\mathbf{x}}_t^{1:N}$, i.e.,

$$\bar{\mathbf{x}}_t^n \sim p(\mathbf{x}_t|\vec{u}, \mathbf{x}_{t-1}^n), \quad n = 1, 2, \dots, N, \quad (22)$$

where $\{\mathbf{x}_{t-1}^n\}_{n=1}^N$ are N equally weighted particles generated from $q(\mathbf{x}_{t-1}|\vec{u})$. With the predicted samples $\bar{\mathbf{x}}_t^{1:N}$, we thus can approximate the prediction distribution as a Gaussian:

$$\begin{aligned} p(\mathbf{x}_t|\vec{u}, \mathbf{y}_{1:t-1}) &= \int p(\mathbf{x}_t|\vec{u}, \mathbf{x}_{t-1})p(\mathbf{x}_{t-1}|\vec{u}, \mathbf{y}_{1:t-1})d\mathbf{x}_{t-1} \\ &= \int p(\mathbf{x}_t|\vec{u}, \mathbf{x}_{t-1})q(\mathbf{x}_{t-1}|\vec{u})d\mathbf{x}_{t-1} \\ &\approx \mathcal{N}(\mathbf{x}_t \mid \bar{\mathbf{m}}_t, \bar{\mathbf{P}}_t) \end{aligned} \quad (23)$$

where $\bar{\mathbf{m}}_t$ and $\bar{\mathbf{P}}_t$ can be computed using Eq. (11). Similarly, during the update step, utilizing Eqs. (13) and (14), we

can derive the variational distribution (approximate posterior distribution) at time step t ,

$$q(\mathbf{x}_t|\vec{\mathbf{u}}) \triangleq p(\mathbf{x}_t|\vec{\mathbf{u}}, \mathbf{y}_{1:t}) = \mathcal{N}(\mathbf{x}_t|\mathbf{m}_t, \mathbf{P}_t) \quad (24)$$

and obtain the set of N updated samples $\mathbf{x}_t^{1:N}$. Note that in the context of GPSSMs, both the prediction and update steps rely on conditioning on the inducing points, which act as a surrogate for the transition function.

So far, we have introduced the utilization of EnKF to obtain the approximate posterior distribution, $q(\mathbf{x}_t|\vec{\mathbf{u}})$. However, in order to evaluate the ELBO and compute term 1 and term 4 in Eq. (21), we still need to determine the conditional distribution, $q(\mathbf{x}_t|\vec{\mathbf{u}}, \mathbf{x}_{t-1})$. Despite having that

$$q(\mathbf{x}_t|\vec{\mathbf{u}}) = \int q(\mathbf{x}_t|\vec{\mathbf{u}}, \mathbf{x}_{t-1})q(\mathbf{x}_{t-1}|\vec{\mathbf{u}})d\mathbf{x}_{t-1}, \quad (25)$$

and both approximations $q(\mathbf{x}_t|\vec{\mathbf{u}})$ and $q(\mathbf{x}_{t-1}|\vec{\mathbf{u}})$ being Gaussian, determining the functional form of a common posterior transition $q(\mathbf{x}_t|\vec{\mathbf{u}}, \mathbf{x}_{t-1}) = p(\mathbf{x}_t|\mathbf{x}_{t-1}, \vec{\mathbf{u}}, \mathbf{y}_{1:t}), \forall t$, remains a challenging task. Therefore, alternative approximation methods are required to efficiently evaluate the ELBO. One alternative manner is to let $q(\mathbf{x}_t|\vec{\mathbf{u}}, \mathbf{x}_{t-1}) = p(\mathbf{x}_t|\vec{\mathbf{u}}, \mathbf{x}_{t-1})$, we then end up with the same ELBO as in [26], where no filtering or smoothing is feasible. To circumvent this limitation, we examine the difference between term 1 and term 4 in Eq. (21) and propose our EnKF-aided variational approximation. The main result is summarized in the following proposition.

Proposition 1. *Under the approximations that, $q(\mathbf{x}_t|\vec{\mathbf{u}}) = p(\mathbf{x}_t|\vec{\mathbf{u}}, \mathbf{y}_{1:t}), \forall t$, and, $p(\mathbf{x}_{t-1}|\vec{\mathbf{u}}, \mathbf{y}_{1:t}) \approx p(\mathbf{x}_{t-1}|\vec{\mathbf{u}}, \mathbf{y}_{1:t-1})$, the difference between term 1 and term 4 in Eq. (21) approximately corresponds to the expected log-likelihood, i.e.,*

$$\text{term1} - \text{term4} \approx \mathbb{E}_{q(\vec{\mathbf{u}})} [\log p(\mathbf{y}_{1:T}|\vec{\mathbf{u}})] \quad (26)$$

Proof. The proof can be found in Appendix A \square

Proposition 1 establishes that computing the expected log-likelihood yields an approximation to the difference between term 1 and term 4, thus the ELBO in Eq. (21) can be approximately evaluated as:

$$\mathcal{L} \approx \mathbb{E}_{q(\vec{\mathbf{u}})} \left[\sum_{t=1}^T \log p(\mathbf{y}_t|\vec{\mathbf{u}}, \mathbf{y}_{1:t-1}) \right] - \text{KL}[q(\mathbf{x}_0)\|p(\mathbf{x}_0)] \quad (27)$$

$$- \text{KL}[q(\vec{\mathbf{u}})\|p(\vec{\mathbf{u}})],$$

where the log-likelihood, $\log p(\mathbf{y}_t|\vec{\mathbf{u}}, \mathbf{y}_{1:t-1})$, at each step t can be analytically evaluated by leveraging the Gaussian prediction distribution, see Eq. (23), and the linear emission model, i.e.,

$$\begin{aligned} \log p(\mathbf{y}_t|\vec{\mathbf{u}}, \mathbf{y}_{1:t-1}) &= \log \int p(\mathbf{y}_t|\mathbf{x}_t)p(\mathbf{x}_t|\vec{\mathbf{u}}, \mathbf{y}_{1:t-1})d\mathbf{x}_t \quad (28) \\ &= \log \mathcal{N}(\mathbf{y}_t|\mathbf{C}\bar{\mathbf{m}}_t, \mathbf{C}\bar{\mathbf{P}}_t\mathbf{C}^\top), \end{aligned}$$

and the KL divergence terms can be analytically computed in closed form [2], due to the Gaussian nature of the prior and variational distributions. Together with all, we can first sample $\vec{\mathbf{u}} \sim q(\vec{\mathbf{u}})$ and numerically get an unbiased evaluation of \mathcal{L} . Thanks to the reparametrization trick [31], we then can apply gradient-based methods [47] to maximize the lower

Algorithm 1 EnKF-aided variational learning and inference

Input: $\theta = [\theta_{gp}, \mathbf{Q}, \mathbf{R}]$, ζ , $\mathbf{y}_{1:T}$, $\mathbf{x}_0^{1:N} \sim q(\mathbf{x}_0)$

- 1: **while** iterations not terminated **do**
- 2: $\vec{\mathbf{u}} \sim q(\vec{\mathbf{u}})$, $L_\ell = 0$
- 3: **for** $t = 1, \dots, T$ **do**
- 4: Get prediction samples using Eq. (22)
- 5: Get empirical moments $\bar{\mathbf{m}}_t, \bar{\mathbf{P}}_t$ using Eq. (23)
- 6: Get Kalman gain: $\bar{\mathbf{G}}_t = \bar{\mathbf{P}}_t \mathbf{C}^\top (\mathbf{C} \bar{\mathbf{P}}_t \mathbf{C}^\top + \mathbf{R})^{-1}$
- 7: Get updated samples using Eq. (14)
- 8: Evaluate the log-likelihood using Eq. (28), and
- 9: $L_\ell = L_\ell + \log p(\mathbf{y}_t|\vec{\mathbf{u}}, \mathbf{y}_{1:t-1})$
- 10: **end for**
- 11: $\mathcal{L} = L_\ell - \text{KL}(q(\mathbf{x}_0)\|p(\mathbf{x}_0)) - \text{KL}(q(\vec{\mathbf{u}})\|p(\vec{\mathbf{u}}))$
- 12: Maximize \mathcal{L} and update θ, ζ using Adam [47]
- 13: **end while**

Output: EnKF particles $\mathbf{x}_{0:T}^{1:N}$, model parameters θ , and variational parameters ζ .

bound \mathcal{L} w.r.t. the model parameters $\theta = [\theta_{gp}, \mathbf{Q}, \mathbf{R}]$ and the variational parameters $\zeta = [\mathbf{m}_0, \mathbf{L}_0, \mathbf{m}, \mathbf{S}, \vec{\mathbf{z}}]$. The pseudo code for implementing the EnKF-aided variational learning and inference algorithm, termed as EnVI, is summarized in Algorithm 1.

The analytical evaluation of the ELBO, \mathcal{L} , as illustrated in Eq. (27), circumvents the explicit evaluation of the first and fourth terms in Eq. (21), and sidesteps the optimization challenge posed by the parameterized $q(\mathbf{x}_t|\vec{\mathbf{u}}, \mathbf{x}_{t-1})$. Consequently, EnVI substantially improves the efficiency of model learning and inference. In addition, maximizing the ELBO in Eq. (27) can be interpreted as follows: The objective is to optimize the model parameters and variational parameters such that the GPSSM can fit the observed data well at each step (indicated by the first term); simultaneously, the KL regularization terms impose constraints to prevent model overfitting (indicated by the second and third terms).

Remark 2 (Computational Complexity of EnVI). *When the dimensionality of the latent state exceeds that of the observation dimension, i.e., $d_x > d_y$, the computational complexity of the EnVI algorithm predominantly lies in the evaluation of N independent particles on the GP transition during the prediction step (cf. (22)). Recall that the number of inducing points is significantly smaller than the length of the data sequence, i.e., $M \ll T$, and assume that $M \geq d_x$. In this context, the computational complexity of Algorithm 1 scales as $\mathcal{O}(NTd_xM^2)$. However, the computation of the N particles on the GP transition can be run in parallel [43], which results in the computational complexity in real-world deployments scaling as $\mathcal{O}(Td_xM^2)$.*

C. More Discussions and Insights

We next provide a comprehensive rationale for selecting EnKF as the integral component of EnVI. We also present detailed insights into the EnVI and discuss its connections to existing works.

Indeed, there are various well-established model-based filtering and smoothing techniques that can be potentially integrated into the variational inference framework for GPSSMs. Such as KF, EKF, PF, and EnKF, to name a few [1]. Among these options, EnKF, as a Monte Carlo-based method, exhibits superior capability in handling nonlinear systems when compared to KF and EKF [44]. While analytical solutions can be obtained for nonlinear systems using e.g. EKF methods, they do not align with the principle advocated by John Tukey that *an approximate solution to the right problem is worth more than a precise solution to the wrong problem* [48]. In comparison to PF, EnKF may have certain limitations in dealing with strongly nonlinear and non-Gaussian systems. However, sampling in PF is generally more computationally demanding, particularly for high-dimensional systems [49], whereas EnKF can be effectively employed even in extremely high-dimensional systems [50]. Moreover, the differentiability of each operation within EnKF allows the EnVI to jointly update the parameters θ and ζ through using modern automatic differentiation tools [43]. In contrast, PF involves resampling from discrete distributions [51], which pose challenges for the utilization of the reparameterization trick [31], [52], resulting in significantly higher computational complexity for gradient computations [53].

It is also vital to emphasize that the proposed EnVI algorithm falls under the NMF category (see definition in Appendix C), given the mutual coupling between the latent state trajectory and the transition function, as evident in the variational distribution, $q(\mathbf{x}_t|\vec{\mathbf{u}})$ in Eq. (24). This indicates that EnVI inherits the favorable characteristics of NMF algorithms [26], which have the potential to enhance learning accuracy and address the issue of underestimating state inference uncertainty, commonly encountered in MF algorithms [32].

Last but not least, note that research work has been conducted on learning dynamical systems using EnKF, as evidenced by works such as [53]–[55] and the references therein. However, it is crucial to emphasize that the proposed EnVI deviates from existing methods in two fundamental aspects.

First, the inherent differentiability of EnVI, spanning from parameters ($\{\theta, \zeta\}$) to latent states and extending to the objective function (the ELBO), enables principled joint learning of dynamics and inference of latent states using automatic differentiation tools such as PyTorch [43]. Most existing methods employ the expectation-maximization (EM) algorithm [2], [56] to iteratively update the model parameters θ and latent state trajectory $\vec{\mathbf{x}}$. However, it has been reported that these methods disregard the gradient information from the parameters θ to the state trajectory $\vec{\mathbf{x}}$, which can potentially degrade the model's learning performance [53], [56]. In contrast, our method draws inspiration from the state-of-the-art EnKF-based dynamical system learning method, autodifferentiable EnKF (AD-EnKF) [53]. By regarding the latent state trajectory as a function of both the model parameters θ and variational parameters ζ , and by leveraging reparameterization tricks and automatic differentiation, we can jointly optimize these parameters in a principled way, resulting in enhanced performance.

Second, EnVI offers an effective means of mitigating the risk of overfitting. In the state-of-the-art AD-EnKF [53], the

transition function in the SSM is modeled using a deterministic parametric model, specifically a neural network, and the optimization objective function is the logarithm of marginal likelihood of the model, i.e.

$$\mathcal{L}_{\text{AD-EnKF}} = \log p(\mathbf{y}_{1:T}) = \sum_{t=1}^T \log p(\mathbf{y}_t|\mathbf{y}_{1:t-1}). \quad (29)$$

However, maximizing this objective function solely w.r.t. the model parameters can easily lead to the model overfitting. In contrast, our method leverages the Bayesian nonparametric model and the variational inference framework to derive the ELBO, as presented in Eq. (27), from which the additional regularization terms for the initial state and state transition function can effectively mitigate the issue of model overfitting. We defer further discussions to Section VI.

V. OENVI: ONLINE LEARNING AND INFERENCE

In this section, we further explore online setting where data is processed sequentially, one sample at a time. It is within this context that the simultaneous inference of states and nonlinear dynamics in GPSSMs presents significant challenges [57]–[60]. The good news is that our EnVI approach readily lends itself to online learning scenarios. At each time step t , we can naturally maximize the corresponding objective function, denoted as L_{ℓ_t} , given by

$$L_{\ell_t} = \mathbb{E}_{q(\vec{\mathbf{u}})} [\log p(\mathbf{y}_t|\vec{\mathbf{u}}, \mathbf{y}_{1:t-1})] - \text{KL}(q(\vec{\mathbf{u}})\|p(\vec{\mathbf{u}})), \quad (30)$$

in terms of both the model parameters and variational parameters. The pseudocode implementation of online EnVI, termed OEnVI, is summarized in Algorithm 2.

Remark 3. *Analogous to EnVI, the computational complexity of OEnVI scales as $\mathcal{O}(d_x M^2)$ under practical parallel computing environments.*

An interesting insight for maximizing the objective function of OEnVI in Eq. (30) (as well as the EnVI's objective function in Eq. (27)) is that it essentially encourages successful data reconstruction while simultaneously ensuring that the filtering distribution $p(\mathbf{x}_t|\vec{\mathbf{u}}, \mathbf{y}_{1:t})$ and the prediction distribution $p(\mathbf{x}_t|\vec{\mathbf{u}}, \mathbf{y}_{1:t-1})$ do not deviate too far from each other, apart from the regularization of $q(\vec{\mathbf{u}})$. This result is supported by the following proposition.

Proposition 2. *The log-likelihood $\log p(\mathbf{y}_t|\vec{\mathbf{u}}, \mathbf{y}_{1:t-1})$ can be expressed as the difference between two fundamental components: the data reconstruction error term, represented by $\mathbb{E}_{q(\mathbf{x}_t|\vec{\mathbf{u}})} [\log p(\mathbf{y}_t|\mathbf{x}_t)]$, and the KL divergence term between the variational distribution $q(\mathbf{x}_t|\vec{\mathbf{u}}, \mathbf{y}_{1:t})$ and the prediction distribution $p(\mathbf{x}_t|\vec{\mathbf{u}}, \mathbf{y}_{1:t-1})$. That is, an alternative form of the objective function for OEnVI can be expressed as*

$$\begin{aligned} L_{\ell_t} = & \mathbb{E}_{q(\vec{\mathbf{u}})} [\mathbb{E}_{q(\mathbf{x}_t|\vec{\mathbf{u}})} [\log p(\mathbf{y}_t|\mathbf{x}_t)]] \\ & - \mathbb{E}_{q(\vec{\mathbf{u}})} [\text{KL}[q(\mathbf{x}_t|\vec{\mathbf{u}})\|p(\mathbf{x}_t|\vec{\mathbf{u}}, \mathbf{y}_{1:t-1})]] \\ & - \text{KL}[q(\vec{\mathbf{u}})\|p(\vec{\mathbf{u}})] \end{aligned} \quad (31)$$

Proof. The proof can be found in Appendix B \square

Algorithm 2 OEnKF: Online EnVI (Step t)

Input: $\theta = [\theta_{gp}, \mathbf{Q}, \mathbf{R}]$, ζ , \mathbf{y}_t , $\mathbf{x}_{t-1}^{1:N}$

1: **while** iterations not terminated **do**

2: $\vec{\mathbf{u}} \sim q(\vec{\mathbf{u}})$, $L_{\ell_t} = 0$

3: Get prediction samples using Eq. (22)

4: Get empirical moments $\bar{\mathbf{m}}_t$, $\bar{\mathbf{P}}_t$ using Eq. (23)

5: Get Kalman gain: $\bar{\mathbf{G}}_t = \bar{\mathbf{P}}_t \mathbf{C}^\top (\mathbf{C} \bar{\mathbf{P}}_t \mathbf{C}^\top + \mathbf{R})^{-1}$

6: Get updated samples using Eq. (14)

7: Evaluate the objective function

$$L_{\ell_t} = \log p(\mathbf{y}_t | \vec{\mathbf{u}}, \mathbf{y}_{1:t-1}) - \text{KL}(q(\vec{\mathbf{u}}) \| p(\vec{\mathbf{u}}))$$

8: Maximize L_{ℓ_t} and update θ , ζ using Adam [47]

9: **end while**

Output: EnKF particles $\mathbf{x}_t^{1:N}$, model parameters θ , and variational parameters ζ .

The insight in Proposition 2 sheds light on the interplay between data reconstruction and the alignment of filtering and prediction distributions in the EnVI and OEnVI algorithms.

Up to this point, it is worth noting that in contrast to the existing inference network-based variational algorithms [25]–[28], [36], [42], [58], [60], OEnVI is a simple and straightforward extension of EnVI, which benefits from eliminating the dependence on amortized inference networks. Previous works have typically employed inference networks that take the entire sequence of observations $\mathbf{y}_{1:T}$ as input, necessitating a significant amount of data for offline training. While it is conceivable to limit the input length of the inference network to a shorter sequence l , such as $\mathbf{y}_{t-l:t}$, this approach still leads to prolonged training times and higher computational requirements for optimizing the inference network parameters [60]. Moreover, storing historical inputs $\mathbf{y}_{t-l:t}$ adds to the storage overhead, making it problematic in situations where historical data duplication and storage are not permissible. In sharp contrast, OEnVI successfully overcomes the aforementioned challenges related to the storage and optimization of inference networks. As a result, it facilitates more efficient learning and inference processes, contributing to improved overall performance. Furthermore, OEnVI offers a more comprehensive objective by simultaneously minimizing the KL divergence, accounting for data reconstruction error balance, and applying regularization to the transition function to mitigate model overfitting. This stands in contrast to the existing approaches that sorely minimize the KL divergence between filtering and prediction distributions in the context of online learning [59].

VI. EXPERIMENTS AND RESULTS

This section presents a comprehensive numerical study of the proposed EnVI and OEnVI. Section VI-A showcases the filtering performance. In Section VI-B, we present the system dynamics learning performance. The series forecasting performance of EnVI on various real datasets is illustrated in Section VI-C. Finally, Section VI-D provides a comprehensive demonstration of the performance of the OEnVI online algorithm. More details regarding the experimental setup can

be found in supplementary material, and the accompanying source code is publicly available online².

A. Learning and Inference in Linear Gaussian SSMs

We investigate the learning and inference capacity of EnVI and OEnVI, by using a linear Gaussian state-space model (LGSSM) where exact inference of latent state is applicable (i.e. KF). Specifically, we use the following LGSSM, a car tracking example given in the textbook [1], to generate observation data, $\mathbf{y}_{1:T}$, for training EnVI and OEnVI,

$$\mathbf{x}_t = \mathbf{H} \mathbf{x}_{t-1} + \mathbf{v}_{t-1}, \quad \mathbf{v}_{t-1} \sim \mathcal{N}(\mathbf{0}, \mathbf{Q}), \quad (32a)$$

$$\mathbf{y}_t = \mathbf{C} \mathbf{x}_t + \mathbf{e}_t, \quad \mathbf{e}_t \sim \mathcal{N}(\mathbf{0}, \mathbf{R}), \quad (32b)$$

where the state and the observation are both four dimensional, and $\mathbf{C} = \mathbf{I}_{4 \times 4}$, $\mathbf{R} = \sigma_R^2 \mathbf{I}_{4 \times 4}$ with $\sigma_R = 0.5$;

$$\mathbf{H} = \begin{pmatrix} 1 & 0 & \Delta t & 0 \\ 0 & 1 & 0 & \Delta t \\ 0 & 0 & 1 & 0 \\ 0 & 0 & 0 & 1 \end{pmatrix} \quad (33)$$

and

$$\mathbf{Q} = \begin{pmatrix} \frac{q_1^c \Delta t^3}{3} & 0 & \frac{q_1^c \Delta t^2}{2} & 0 \\ 0 & \frac{q_2^c \Delta t^3}{3} & 0 & \frac{q_2^c \Delta t^2}{2} \\ \frac{q_1^c \Delta t^2}{2} & 0 & q_1^c \Delta t & 0 \\ 0 & \frac{q_2^c \Delta t^2}{2} & 0 & q_2^c \Delta t \end{pmatrix} \quad (34)$$

with $\Delta t = 0.1$, $q_1^c = q_2^c = 1$.

We begin by generating $T = 120$ training observations. For EnVI, we employ 1000 epochs/iterations for training, but convergence is typically achieved approximately 300 iterations. In OEnVI, the parameters θ and ζ are updated once per time step t . Both EnVI and OEnVI employ 15 inducing points, a setting that will be used for subsequent experiments unless otherwise specified. We report the state inference results, which are depicted in Fig. 2. It can be observed that the state inference performance of EnVI and OEnVI is comparable to that of the KF in terms of state-fitting root mean square error (RMSE), despite being trained solely on noisy observations without any physical model knowledge.

Another finding is that though OEnVI incurs a lower training cost compared to EnVI, this advantage comes at the expense of inadequate learning of the latent dynamics, leading to a less accurate estimation of the latent states when compared to EnVI. The discrepancy is evident in Fig. 2, where OEnVI exhibits larger estimation RMSE and greater estimation uncertainty for the latent states in comparison to EnVI and KF. Notably, EnVI relies on offline training, resulting in an uncertainty quantification that closely approaches the optimal estimate, the KF estimate. Nevertheless, it is essential to mention that, with continuous online data arrival, OEnVI can eventually achieve a comparable state estimation performance as EnVI. We observed that after observing 360 data points, OEnVI achieves a latent state RMSE estimation of 0.6512. Further details on this aspect of the results are provided in the supplementary material (See Supplement B-A).

²<https://github.com/zhidilin/gpssmProj>

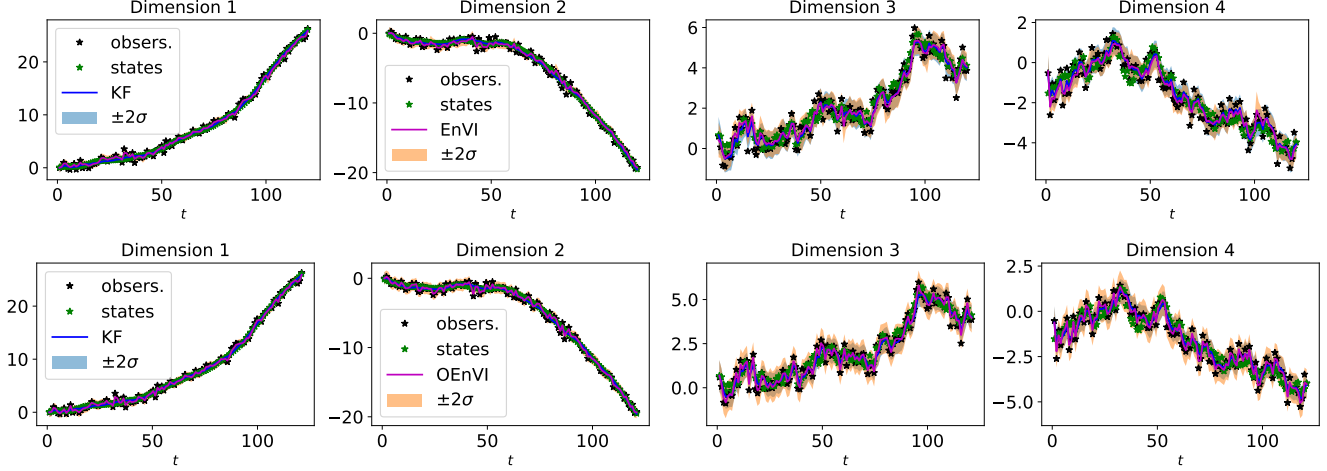


Fig. 2. EnVI (top) & OEnVI (bottom) on state inference in linear Gaussian SSM. The RMSE of the latent state estimates for KF, EnVI, and OEnVI are 0.5252, 0.6841, and 0.7784, respectively; the RMSE between the observations and the latent states is 0.9872.

B. System Dynamics Learning

This subsection demonstrates the superior capability of EnVI in learning latent dynamics for GPSSMs. To evaluate its performance, we utilize a 1-D synthetic dataset called the *kink* function dataset, which is generated from a dynamical system described by Eq. (35), where the nonlinear, smooth and time-invariant function $f(\mathbf{x}_t)$ is called the “*kink*” function,

$$\mathbf{x}_{t+1} = 0.8 + (\mathbf{x}_t + 0.2) \underbrace{\left[1 - \frac{5}{1 + \exp(-2\mathbf{x}_t)} \right]}_{\triangleq \text{“kink function” } f(\mathbf{x}_t)} + \mathbf{v}_t, \quad (35a)$$

$$\mathbf{y}_t = \mathbf{x}_t + \mathbf{e}_t, \quad \mathbf{v}_t \sim \mathcal{N}(0, \sigma_Q^2), \quad \mathbf{e}_t \sim \mathcal{N}(0, \sigma_R^2). \quad (35b)$$

It is worth mentioning that this specific dynamical system has been extensively employed in GPSSM literature to evaluate the accuracy of the learned GP transition posterior [29].

In showcasing the superior performance of EnVI, we compare it against several prominent competing methods, namely vGPSSM [25], VCDT [27], and AD-EnKF [53]. Our implementation of VCDT incorporates an amortized inference network to address the linear growth in the number of variational parameters. The vGPSSM method adheres to the original paper’s implementation [25], while the AD-EnKF is utilized as per the default software package available online³. The training data sequences are generated by fixing σ_Q^2 at 0.05 and systematically vary σ_R^2 within the range of {0.008, 0.08, 0.8}. As a result, we generate three sets of $T = 600$ observations each for training. To ensure a fair comparison in the latent space, we adhere to Ialongo *et al.* [27] and keep the emission model fixed to the true generative ones for all methods, while allowing the transition to be learned. Further details, including the description of the setup for the aforementioned algorithms, are provided in Supplement B-B and the accompanying source code. The result is depicted in Table I and visualized in Fig. 3. We can find that EnVI consistently outperforms existing approaches in terms of the latent dynamic learning performance and robustness. We next conduct two ablation studies.

EnVI vs. Inference Network-Based Methods. Based on the numerical results presented in Table I, we can find that the EnVI exhibits superior dynamic learning performance compared to vGPSSM and VCDT, both of which rely on an inference network. Specifically, as illustrated in Fig. 3, vGPSSM faces more challenges in dynamic learning, while VCDT, categorized under the NMF paradigm, only performs well under more minor noise conditions ($\sigma_R^2 = 0.008$ and $\sigma_R^2 = 0.08$). In contrast, EnVI effectively learns the GP transition well, even in the high noise setting with $\sigma_R^2 = 0.8$.

The primary reason for this discrepancy is the increased complexity arising from additional inference network parameters, which hinder effective training. Furthermore, the inference network-based methods are prone to convergence into various unfavorable local optima, demonstrating reduced robustness. As a consequence, the learning performance of such methods often fluctuates significantly. In contrast, EnVI inherits the benefits of EnKF and avoids the need to optimize additional variational parameters from the inference network, making it more amenable to optimization and demonstrating enhanced robustness. Our experimental findings consistently demonstrate that EnVI exhibits faster convergence compared to vGPSSM and VCDT. For instance, when considering $\sigma_R^2 = 0.008$, EnVI achieves convergence after 300 iterations, while both vGPSSM and VCDT require more iterations, as shown in Fig. 4.

EnVI vs. AD-EnKF. The primary difference between EnVI and AD-EnKF lies in their data-driven modules. AD-EnKF employs a parametric model, specifically a neural network (so it is known as a deep SSM (DSSM)), while EnVI utilizes a nonparametric GP. Consequently, the dynamics learned by AD-EnKF exhibit a tendency to be over-confident, as depicted in Fig. 3, as it does not account for uncertainties from the learned transition function. Moreover, the absence of regularization during the training of the neural network in AD-EnKF (as indicated in Eq. (29)) renders the method susceptible to overfitting and being trapped in suboptimal solutions during the training process. As a result, the performance of different repetitions can vary significantly, as shown in Table I.

³<https://github.com/ymchen0/torchEnKF>

TABLE I

COMPARISON OF OUR METHOD WITH OTHER COMPETITORS ON THE KINK FUNCTION DATASET. SHOWN ARE MEAN AND STANDARD ERRORS OVER FIVE REPETITIONS OF THE FITTING MSE (LOWER IS BETTER) AND THE LOG-DENSITY (HIGHER IS BETTER) OF THE KINK FUNCTION VARYING THE EMISSION NOISE VARIANCE σ_R^2 .

Method	$\sigma_R^2 = 0.008$ (MSE Log-Likelihood)	$\sigma_R^2 = 0.08$ (MSE Log-Likelihood)	$\sigma_R^2 = 0.8$ (MSE Log-Likelihood)
vGPSSM [25]	1.0410 ± 0.7426 -27.5981 ± 19.7817	1.6390 ± 0.6783 -30.9557 ± 16.9218	1.9584 ± 0.9655 -56.5997 ± 37.8221
VCDT [27]	0.2057 ± 0.2219 -1.058 ± 1.5005	0.1934 ± 0.0140 -0.5867 ± 0.2610	1.4035 ± 0.6470 -3.8092 ± 0.6588
AD-EnKF [53]	0.0285 ± 0.0318 -3.6282 ± 6.3514	1.5246 ± 0.9734 -242.2795 ± 194.6741	1.3489 ± 0.3102 -267.7068 ± 62.0488
EnVI (ours)	0.0046 ± 0.0025 1.1060 ± 0.0381	0.0536 ± 0.0232 0.1025 ± 0.1075	0.5315 ± 0.1542 -1.0439 ± 0.1714

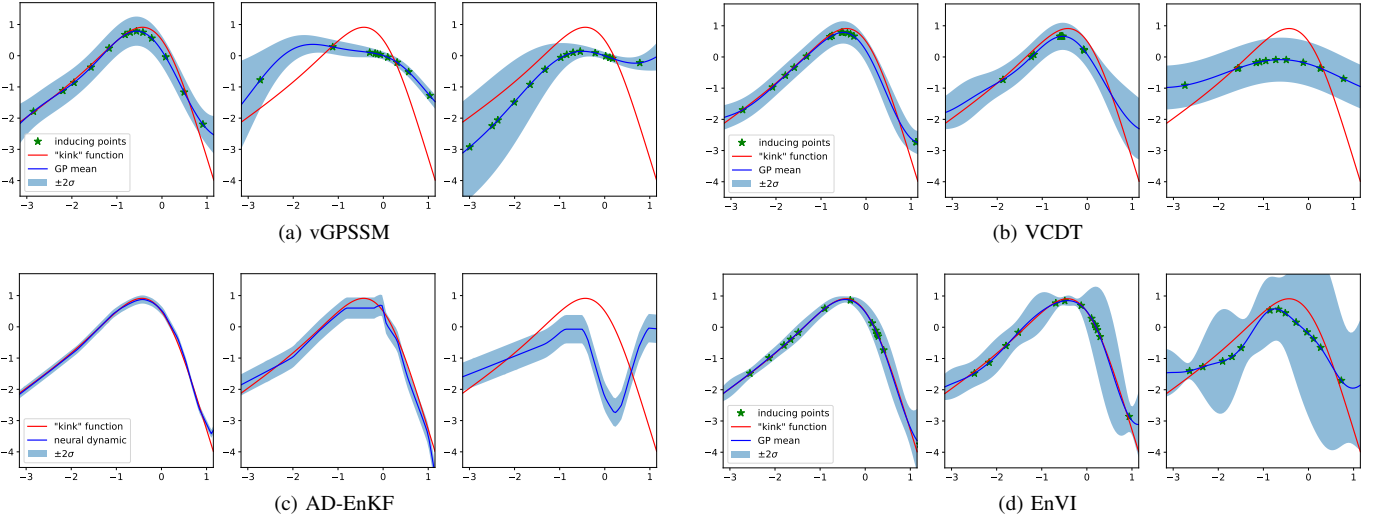


Fig. 3. Kink transition function learning performance (mean $\pm 2\sigma$) using various methods across different levels of emission noise ($\sigma_R^2 \in \{0.008, 0.08, 0.8\}$, from left to right).

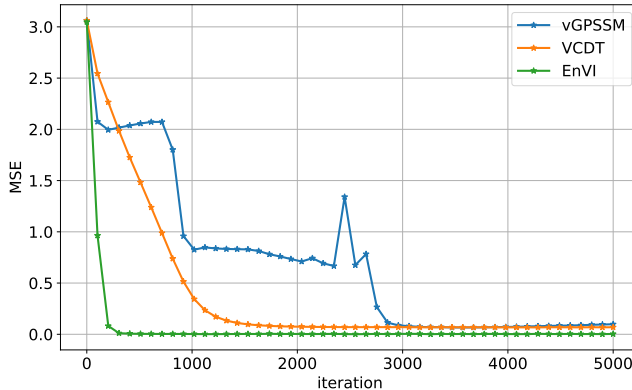


Fig. 4. Kink function learning performance against the training iterations. EnVI exhibits faster convergence compared to vGPSSM and VCDT.

C. Time Series Data Forecasting

This subsection demonstrates the series prediction performance of the proposed EnVI algorithm on five public real-world system identification datasets⁴, which consist of one-dimensional time series of varying lengths between 296 to 1024 data points. In addition to the comparison methods discussed in Section VI-B, EnVI is also compared with several other competitors, including two NMF class methods, PRSSM [26], ODGPSSM [35], and two inference network-based methods, DKF [42] and CO-GPSSM [36], as depicted

in Table II. For each method's training, the first half of the sequence in every dataset is utilized as training data, with the remaining portion designated for testing. Standardization of all datasets is conducted based on the training sequence, and the latent state dimension, d_x , is consistently set to 4 for all datasets. Table II reports the series prediction results, wherein the RMSE is averaged over 50-step ahead forecasting.

Table II reveals that EnVI outperforms almost all approaches across five datasets. Specifically, EnVI demonstrates superior performance among the MF and NMF methods. Compared to PRSSM and ODGPSSM [26], [35], which assume equality between variational and prior distributions of latent states, EnVI employs EnKF to filter latent states, leading to an enhanced system dynamics learning performance, and consequently, improving the series predictions. Compared to the inference network-based methods, like VCDT [27] and the MF class methods vGPSSM [25] and CO-GPSSM [36], EnVI eliminates the need to optimize inference network parameters. From an optimization solution perspective, optimizing the inference network leads to a vast solution space for the variational distribution. Consequently, despite their adequate approximation capabilities for the true posterior distribution, these inference network-based methods often fall short of realizing their theoretical potential in empirical performance due to numerous bad local optima [29]. In contrast, EnVI imposes model-based constraints on the variational distribution by the EnKF, narrowing the solution space and yielding significantly improved and robust empirical performance.

⁴<https://homes.esat.kuleuven.be/~smc/daisy/daisydata.html>

TABLE II
PREDICTION PERFORMANCE (RMSE) OF THE DIFFERENT MODELS ON THE SYSTEM IDENTIFICATION DATASETS. MEAN AND STANDARD DEVIATION OF THE PREDICTION RESULTS ARE SHOWN ACROSS FIVE SEEDS. THE TOP THREE RESULTS ARE HIGHLIGHTED IN BOLD.

Category	Method	Actuator	Ball Beam	Drive	Dryer	Gas Furnace
DSSMs	DKF [42]	1.204 \pm 0.250	0.144 \pm 0.005	0.735 \pm 0.001	1.465 \pm 0.087	5.589 \pm 0.066
	AD-EnKF [53]	0.705 \pm 0.117	0.057 \pm 0.006	0.756 \pm 0.114	0.182 \pm 0.053	1.408 \pm 0.090
MF-based Methods	vGPSSM [25]	1.640 \pm 0.011	0.268 \pm 0.414	0.740 \pm 0.010	0.822 \pm 0.002	3.676 \pm 0.145
	CO-GPSSM [36]	0.803 \pm 0.011	0.079 \pm 0.018	0.736 \pm 0.007	0.366 \pm 0.146	1.898 \pm 0.157
NMF-based Methods	PRSSM [26]	0.691 \pm 0.148	0.074 \pm 0.010	0.647 \pm 0.057	0.174 \pm 0.013	1.503 \pm 0.196
	ODGPSSM [35]	0.666 \pm 0.074	0.068 \pm 0.006	0.708 \pm 0.052	0.171 \pm 0.011	1.704 \pm 0.560
	VCDT [27]	0.815 \pm 0.012	0.065 \pm 0.005	0.735 \pm 0.005	0.667 \pm 0.266	2.052 \pm 0.163
	EnVI (ours)	0.657 \pm 0.095	0.055 \pm 0.002	0.703 \pm 0.050	0.125 \pm 0.017	1.388 \pm 0.123

Compared to the DSSM methods, EnVI offers performance advantages due to its non-parametric GP model. In contrast to DKF [42], which utilizes neural networks to model variational distributions and nonlinear SSMs, EnVI employs GPs with much less model parameters, making it particularly suitable for small datasets. While AD-EnKF [53] outperforms DKF, its deterministic neural network modeling approach, and absence of regularization in its objective function cause it to lag behind EnVI in forecasting performance.

D. Online Learning and Inference with OEnVI

We next evaluate the performance of OEnVI. We compare OEnVI with two very recent competitive online learning algorithms, specifically SVMC [58], which models the variational distribution of latent states using sample particles, and VJF [60], where the variational distribution of latent states is modeled by an inference network. More numerical results of OEnVI about learning kink dynamical function can be found in Supplement B-D.

We evaluate the three online learning methods using NASCAR® data, a dataset previously utilized in [58], showcasing dynamics akin to recurrent switching linear dynamical systems [61]. The simulated trajectory faithfully reproduces the layout of a NASCAR® track, as depicted in Fig. 5a. We train these three methods with 2000 observations and test them with 500 observations, both simulated from $\mathbf{y}_t = \mathbf{C}\mathbf{x}_t + \mathbf{e}_t$ where \mathbf{C} is a 10-by-2 matrix generated randomly. The SVMC and VJF algorithms are implemented using the code publicly provided online⁵⁶.

Figs. 5a–5c depict the true states (in blue) and the latent states (in red) inferred by the three methods. The results clearly indicate that EnVI and SVMC swiftly captured the real state and maintained accuracy, while VJF faced challenges, primarily due to its difficulty in learning the inference network. A detailed comparison with SVMC, as illustrated in Figs. 5d–5f, underscores EnVI’s superior accuracy in both inference and prediction of latent states. These empirical findings emphasize OEnVI’s efficacy, particularly in its use of EnKF to approximate the variational distribution, demonstrating its advancement over VJF using inference networks, and SVMC using PF methods.

⁵<https://github.com/catniplab/svmc>

⁶<https://github.com/catniplab/vjf>

VII. CONCLUSION AND FUTURE WORK

In this paper, we have introduced EnVI, a novel NMF algorithm tailored for GPSSMs, which integrates EnKF into a variational inference framework. Additionally, we have presented an extended online version, OEnVI. Both algorithms eliminate the necessity for inference networks and shape the variational distribution over latent states through model-based EnKF, enhancing model training efficiency and algorithm robustness compared to existing methods. Empirical experiments conducted on diverse real and synthetic datasets, evaluating filtering, prediction, and dynamics learning performance, unequivocally support the effectiveness of the proposed methods. Looking ahead, our focus is on further reducing the computational complexity of the GP transition function and enhancing its modeling capacity. This effort aims to render the GPSSM compatible with more high-dimensional datasets, aligning it with the capabilities of EnKF and enabling the application of EnVI in more practical, high-dimensional dynamic systems.

APPENDIX A

PROOF OF PROPOSITION 1

Proof. The proof is shown as follows,

term 1 – term 4

$$= \mathbb{E}_{q(\vec{\mathbf{u}}, \vec{\mathbf{x}})} \left[\sum_{t=1}^T \log \frac{p(\mathbf{y}_t | \mathbf{x}_t) p(\mathbf{x}_t | \vec{\mathbf{u}}, \mathbf{x}_{t-1})}{q(\mathbf{x}_t | \vec{\mathbf{u}}, \mathbf{x}_{t-1})} \right] \quad (36a)$$

$$= \mathbb{E}_{q(\vec{\mathbf{u}}, \vec{\mathbf{x}})} \left[\sum_{t=1}^T \log \frac{p(\mathbf{y}_t | \mathbf{x}_t) p(\mathbf{x}_t | \vec{\mathbf{u}}, \mathbf{x}_{t-1}) q(\mathbf{x}_{t-1} | \vec{\mathbf{u}})}{q(\mathbf{x}_t | \vec{\mathbf{u}}, \mathbf{x}_{t-1}) q(\mathbf{x}_{t-1} | \vec{\mathbf{u}})} \right] \quad (36b)$$

$$\approx \mathbb{E}_{q(\vec{\mathbf{u}}, \vec{\mathbf{x}})} \left[\sum_{t=1}^T \log \frac{p(\mathbf{y}_t | \mathbf{x}_t) p(\mathbf{x}_t | \vec{\mathbf{u}}, \mathbf{x}_{t-1}) q(\mathbf{x}_{t-1} | \vec{\mathbf{u}})}{q(\mathbf{x}_t | \vec{\mathbf{u}}, \mathbf{x}_{t-1}) p(\mathbf{x}_{t-1} | \vec{\mathbf{u}}, \mathbf{y}_{1:t})} \right] \quad (36c)$$

$$= \mathbb{E}_{q(\vec{\mathbf{u}}, \vec{\mathbf{x}})} \left[\sum_{t=1}^T \log \frac{p(\mathbf{y}_t, \mathbf{x}_t, \mathbf{x}_{t-1} | \vec{\mathbf{u}}, \mathbf{y}_{1:t-1})}{p(\mathbf{x}_t, \mathbf{x}_{t-1} | \vec{\mathbf{u}}, \mathbf{y}_{1:t-1}, \mathbf{y}_t)} \right] \quad (36d)$$

$$= \mathbb{E}_{q(\vec{\mathbf{u}})} \left[\sum_{t=1}^T \log p(\mathbf{y}_t | \vec{\mathbf{u}}, \mathbf{y}_{1:t-1}) \right] \quad (36e)$$

$$= \mathbb{E}_{q(\vec{\mathbf{u}})} [\log p(\mathbf{y}_{1:T} | \vec{\mathbf{u}})]. \quad (36f)$$

where Eq. (36c) holds because of the approximation of $p(\mathbf{x}_{t-1} | \vec{\mathbf{u}}, \mathbf{y}_{1:t}) \approx p(\mathbf{x}_{t-1} | \vec{\mathbf{u}}, \mathbf{y}_{1:t-1})$ and Eq. (36e) is derived straightforwardly by applying Bayes’ theorem. \square

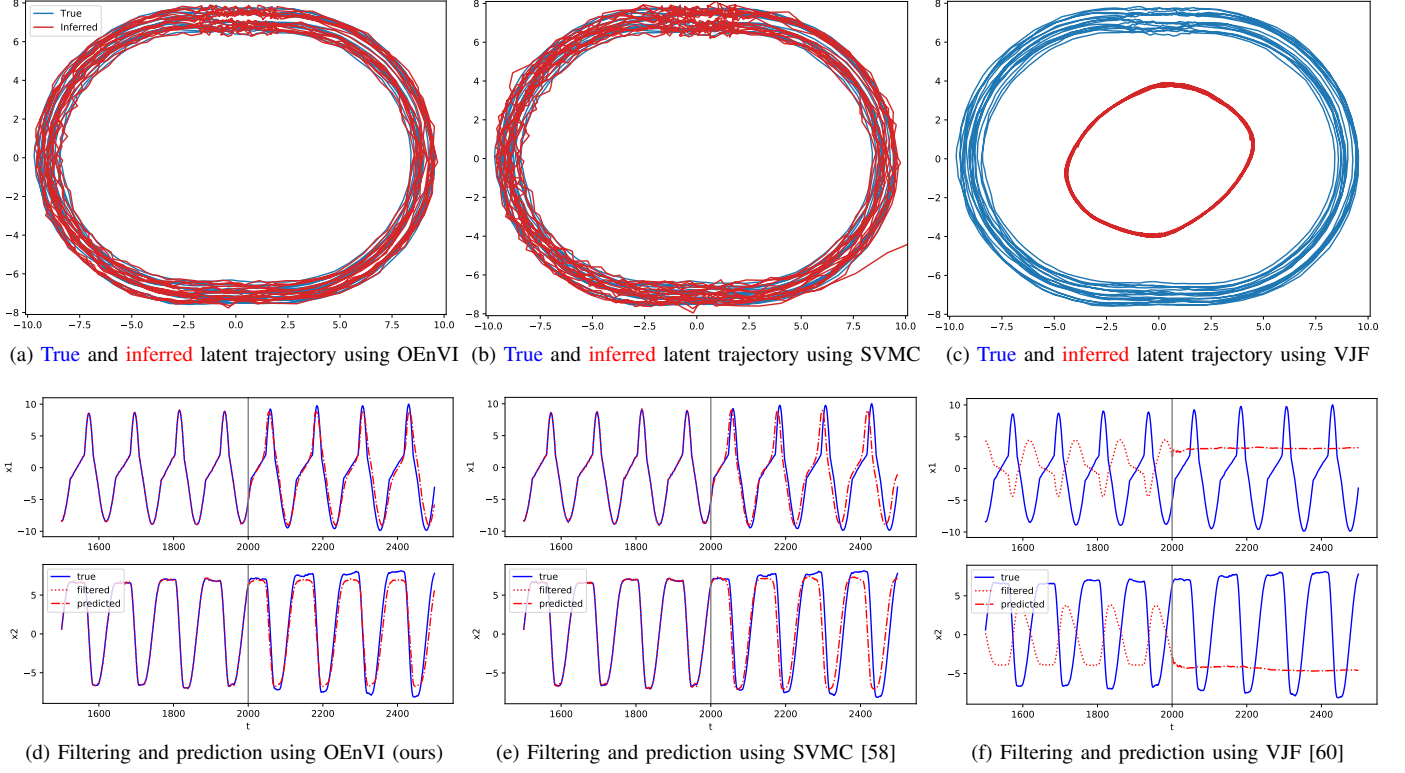


Fig. 5. Online NASCAR® dynamics learning results of the three online methods [61]

APPENDIX B

PROOF OF PROPOSITION 2
Proof. Under the approximation that $q(\mathbf{x}_t|\vec{\mathbf{u}}) \triangleq p(\mathbf{x}_t|\vec{\mathbf{u}}, \mathbf{y}_{1:t})$, we have the log-likelihood term

$$\log p(\mathbf{y}_t|\vec{\mathbf{u}}, \mathbf{y}_{1:t-1}) \quad (37a)$$

$$= \mathbb{E}_{p(\mathbf{x}_t|\vec{\mathbf{u}}, \mathbf{y}_{1:t})} [\log p(\mathbf{y}_t|\vec{\mathbf{u}}, \mathbf{y}_{1:t-1})] \quad (37b)$$

$$= \mathbb{E}_{p(\mathbf{x}_t|\vec{\mathbf{u}}, \mathbf{y}_{1:t})} \left[\log \frac{p(\mathbf{x}_t|\vec{\mathbf{u}}, \mathbf{y}_{1:t-1})p(\mathbf{y}_t|\mathbf{x}_t)}{p(\mathbf{x}_t|\vec{\mathbf{u}}, \mathbf{y}_{1:t-1}, \mathbf{y}_t)} \right] \quad (37c)$$

$$= -\mathbb{E}_{p(\mathbf{x}_t|\vec{\mathbf{u}}, \mathbf{y}_{1:t})} \left[\log \frac{p(\mathbf{x}_t|\vec{\mathbf{u}}, \mathbf{y}_{1:t})}{p(\mathbf{x}_t|\vec{\mathbf{u}}, \mathbf{y}_{1:t-1})p(\mathbf{y}_t|\mathbf{x}_t)} \right] \quad (37d)$$

$$= -\text{KL} [p(\mathbf{x}_t|\vec{\mathbf{u}}, \mathbf{y}_{1:t}) \| p(\mathbf{x}_t|\vec{\mathbf{u}}, \mathbf{y}_{1:t-1})] \quad (37e)$$

$$+ \mathbb{E}_{p(\mathbf{x}_t|\vec{\mathbf{u}}, \mathbf{y}_{1:t})} [\log p(\mathbf{y}_t|\mathbf{x}_t)],$$

which completes the proof. Here Eq. (37c) is obtained straightforwardly by applying Bayes' theorem. \square

APPENDIX C

MEAN-FIELD AND NON-MEAN-FIELD APPROXIMATIONS

Definition 1. If the variational distribution, $q(\vec{\mathbf{f}}, \vec{\mathbf{u}}, \vec{\mathbf{x}})$, is factorized such that the transition function values and the latent states are independent, i.e.,

$$q(\vec{\mathbf{f}}, \vec{\mathbf{u}})q(\mathbf{x}_0) \prod_{t=1}^T q(\mathbf{x}_t|\mathbf{f}_t) = q(\vec{\mathbf{f}}, \vec{\mathbf{u}})q(\vec{\mathbf{x}}), \quad (38)$$

the factorization is known as a mean-field approximation in the GPSSM literature. Conversely, if the variational distribution, $q(\vec{\mathbf{x}}, \vec{\mathbf{f}}, \vec{\mathbf{u}})$, explicitly builds the dependence between the latent states and the transition function values, as shown in Eq. (8), it is a non-mean-field approximation.

REFERENCES

- [1] S. Särkkä, *Bayesian filtering and smoothing*. Cambridge University Press, 2013, no. 3.
- [2] S. Theodoridis, *Machine Learning: A Bayesian and Optimization Perspective*, 2nd ed. Academic Press, 2020.
- [3] C. M. Bishop, *Pattern Recognition and Machine Learning*. Springer, 2006.
- [4] Z. Yan, P. Cheng, Z. Chen, Y. Li, and B. Vucetic, “Gaussian process reinforcement learning for fast opportunistic spectrum access,” *IEEE Trans. Signal Process.*, vol. 68, pp. 2613–2628, Apr. 2020.
- [5] K. Arulkumaran, M. P. Deisenroth, M. Brundage, and A. A. Bharath, “Deep reinforcement learning: A brief survey,” *IEEE Signal Process. Mag.*, vol. 34, no. 6, pp. 26–38, Nov. 2017.
- [6] A. M. Alaa and M. van der Schaar, “Attentive state-space modeling of disease progression,” in *Proc. Adv. Neural Inf. Process. Syst. (NeurIPS)*, Vancouver, BC, Canada, Dec. 2019, pp. 11 338–11 348.
- [7] G. Revach, N. Shlezinger, X. Ni, A. L. Escoriza, R. J. Van Sloun, and Y. C. Eldar, “KalmanNet: Neural network aided Kalman filtering for partially known dynamics,” *IEEE Trans. Signal Process.*, vol. 70, pp. 1532–1547, Mar. 2022.
- [8] R. Frigola, “Bayesian time series learning with Gaussian processes,” Ph.D. dissertation, University of Cambridge, 2015.
- [9] C. E. Rasmussen and C. K. I. Williams, *Gaussian Processes for Machine Learning*. MIT Press, 2006.
- [10] J. M. Wang, D. J. Fleet, and A. Hertzmann, “Gaussian process dynamical models for human motion,” *IEEE Trans. Pattern Anal. Mach. Intell.*, vol. 30, no. 2, pp. 283–298, Dec. 2007.
- [11] R. Turner, M. Deisenroth, and C. Rasmussen, “State-space inference and learning with Gaussian processes,” in *Proc. Int. Conf. Artif. Intell. Stat. (AISTATS)*, Sardinia, Italy, May 2010, pp. 868–875.
- [12] M. P. Deisenroth, D. Fox, and C. E. Rasmussen, “Gaussian processes for data-efficient learning in robotics and control,” *IEEE Trans. Pattern Anal. Mach. Intell.*, vol. 37, no. 2, pp. 408–423, Nov. 2013.
- [13] M. P. Deisenroth, R. D. Turner, M. F. Huber, U. D. Hanebeck, and C. E. Rasmussen, “Robust filtering and smoothing with Gaussian processes,” *IEEE Trans. Autom. Control*, vol. 57, no. 7, pp. 1865–1871, Dec. 2011.

[14] J. Ko and D. Fox, "GP-BayesFilters: Bayesian filtering using Gaussian process prediction and observation models," *Auton. Robots*, vol. 27, no. 1, pp. 75–90, Jul. 2009.

[15] ——, "Learning GP-BayesFilters via Gaussian process latent variable models," *Auton. Robots*, vol. 30, no. 1, pp. 3–23, Oct. 2011.

[16] Y. Zhao, C. Fritzsche, G. Hendeby, F. Yin, T. Chen, and F. Gunnarsson, "Cramér–Rao bounds for filtering based on Gaussian process state-space models," *IEEE Trans. Signal Process.*, vol. 67, no. 23, pp. 5936–5951, Oct. 2019.

[17] A. Xie, F. Yin, B. Ai, S. Zhang, and S. Cui, "Learning while tracking: A practical system based on variational Gaussian process state-space model and smartphone sensory data," in *Proc. Int. Conf. Inf. Fusion (FUSION)*, Rustenburg, South Africa, Jul. 2020, pp. 1–7.

[18] R. Frigola, F. Lindsten, T. B. Schön, and C. E. Rasmussen, "Bayesian inference and learning in Gaussian process state-space models with particle MCMC," in *Proc. Adv. Neural Inf. Process. Syst. (NeurIPS)*, Lake Tahoe, NV, United states, Dec. 2013, pp. 3156–3164.

[19] A. Svensson, A. Solin, S. Särkkä, and T. Schön, "Computationally efficient Bayesian learning of Gaussian process state space models," in *Proc. Int. Conf. Artif. Intell. Stat. (AISTATS)*, Cadiz, Spain, May 2016, pp. 213–221.

[20] A. Svensson and T. B. Schön, "A flexible state-space model for learning nonlinear dynamical systems," *Automatica*, vol. 80, pp. 189–199, Jun. 2017.

[21] K. Berntorp, "Online Bayesian inference and learning of Gaussian-process state-space models," *Automatica*, vol. 129, p. 109613, Jul. 2021.

[22] A. Solin and S. Särkkä, "Hilbert space methods for reduced-rank Gaussian process regression," *Stat. Comput.*, vol. 30, no. 2, pp. 419–446, Mar. 2020.

[23] R. Frigola, Y. Chen, and C. E. Rasmussen, "Variational Gaussian process state-space models," in *Proc. Adv. Neural Inf. Process. Syst. (NeurIPS)*, Montreal, QC, Canada, Dec. 2014, pp. 3680–3688.

[24] A. J. McHutchon, "Nonlinear modelling and control using Gaussian processes," Ph.D. dissertation, University of Cambridge, 2014.

[25] S. Eleftheriadis, T. Nicholson, M. P. Deisenroth, and J. Hensman, "Identification of Gaussian process state space models," in *Proc. Adv. Neural Inf. Process. Syst. (NeurIPS)*, Long Beach, CA, United states, Dec. 2017, pp. 5309–5319.

[26] A. Doerr, C. Daniel, M. Schiegg, N.-T. Duy, S. Schaal, M. Toussaint, and T. Sebastian, "Probabilistic recurrent state-space models," in *Proc. Int. Conf. Mach. Learn. (ICML)*, Stockholm, Sweden, Jul. 2018, pp. 1280–1289.

[27] A. D. Ialongo, M. van der Wilk, J. Hensman, and C. E. Rasmussen, "Overcoming mean-field approximations in recurrent Gaussian process models," in *Proc. Int. Conf. Mach. Learn. (ICML)*, Long Beach, CA, United states, Jun. 2019, pp. 2931–2940.

[28] S. Curi, S. Melchior, F. Berkenkamp, and A. Krause, "Structured variational inference in partially observable unstable Gaussian process state space models," in *Proc. Learning for Dynamics and Control (L4DC)*, Virtual, Online, Jun. 2020, pp. 147–157.

[29] J. Lindinger, B. Rakitsch, and C. Lippert, "Laplace approximated Gaussian process state-space models," in *Proc. Conf. Uncertain. Artif. Intell. (UAI)*, Eindhoven, Netherlands, Aug. 2022.

[30] M. Titsias, "Variational learning of inducing variables in sparse Gaussian processes," in *Proc. Int. Conf. Artif. Intell. Stat. (AISTATS)*, Clearwater, FL, United states, Apr. 2009, pp. 567–574.

[31] D. P. Kingma and M. Welling, "An introduction to variational autoencoders," *Found. Trends Mach. Learn.*, vol. 12, no. 4, pp. 307–392, Nov. 2019.

[32] R. E. Turner and M. Sahani, "Two problems with variational expectation maximisation for time-series models," in *Bayesian Time series models*. Cambridge University Press, 2011, ch. 5, pp. 109–130.

[33] Y. Liu and P. M. Djurić, "Gaussian process state-space models with time-varying parameters and inducing points," in *Proc. European Signal Proces. Conf. (EUSIPCO)*, Amsterdam, Netherlands, Jan. 2021, pp. 1462–1466.

[34] Y. Liu, M. Ajirak, and P. M. Djurić, "Sequential estimation of Gaussian process-based deep state-space models," *IEEE Trans. Signal Process.*, vol. 71, pp. 2968–2980, Aug. 2023.

[35] Z. Lin, L. Cheng, F. Yin, L. Xu, and S. Cui, "Output-dependent Gaussian process state-space model," in *Proc. IEEE Int. Conf. Acoust. Speech Signal Process. (ICASSP)*, Rhodes, Greek, Jun. 2023, pp. 1–5.

[36] Z. Lin, F. Yin, and J. Maroñas, "Towards flexibility and interpretability of Gaussian process state-space model," *arXiv preprint arXiv:2301.08843*, 2023.

[37] Z. Lin, J. Maroñas, Y. Li, F. Yin, and S. Theodoridis, "Towards efficient modeling and inference in multi-dimensional Gaussian process state-space models," *arXiv preprint arXiv:2309.01074*, 2023.

[38] X. Fan, E. V. Bonilla, T. O’Kane, and S. A. Sisson, "Free-form variational inference for Gaussian process state-space models," in *Proc. Int. Conf. Mach. Learn. (ICML)*, Jul. 2023, pp. 9603–9622.

[39] T. Chen, E. Fox, and C. Guestrin, "Stochastic gradient Hamiltonian Monte Carlo," in *Proc. Int. Conf. Mach. Learn. (ICML)*, Beijing, China, Jun. 2014, pp. 1683–1691.

[40] L. Cheng, F. Yin, S. Theodoridis, S. Chatzis, and T.-H. Chang, "Rethinking Bayesian learning for data analysis: The art of prior and inference in sparsity-aware modeling," *IEEE Signal Process. Mag.*, vol. 39, no. 6, pp. 18–52, Nov. 2022.

[41] J. Courts, A. G. Wills, and T. B. Schön, "Gaussian variational state estimation for nonlinear state-space models," *IEEE Trans. Signal Process.*, vol. 69, pp. 5979–5993, Oct. 2021.

[42] R. Krishnan, U. Shalit, and D. Sontag, "Structured inference networks for nonlinear state space models," in *Proc. AAAI Conf. Artif. Intell. (AAAI)*, San Francisco, CA, United states, Feb. 2017, pp. 2101–2109.

[43] A. Paszke, S. Gross, F. Massa, A. Lerer, J. Bradbury, G. Chanan, T. Killeen, Z. Lin, N. Gimelshein, L. Antiga *et al.*, "Pytorch: an imperative style, high-performance deep learning library," in *Proc. Adv. Neural Inf. Process. Syst. (NeurIPS)*, Vancouver, Canada, Dec. 2019, pp. 8026–8037.

[44] M. Roth, G. Hendeby, C. Fritzsche, and F. Gustafsson, "The ensemble Kalman filter: A signal processing perspective," *EURASIP J. Adv. Signal Process.*, vol. 2017, pp. 1–16, Dec. 2017.

[45] J. Hensman, N. Fusi, and N. D. Lawrence, "Gaussian processes for big data," in *Proc. Conf. Uncertain. Artif. Intell. (UAI)*, Bellevue, WA, United states, Jul. 2013, pp. 282–290.

[46] M. D. Hoffman, D. M. Blei, C. Wang, and J. Paisley, "Stochastic variational inference," *J. Mach. Learn. Res.*, vol. 14, no. 40, pp. 1303–1347, May 2013.

[47] D. P. Kingma and J. Ba, "Adam: A method for stochastic optimization," in *Proc. Int. Conf. Learn. Represent. (ICLR)*, San Diego, CA, United states, May 2015.

[48] J. W. Tukey, "The future of data analysis," *Ann. Math. Stat.*, vol. 33, no. 1, pp. 1–67, Mar. 1962.

[49] C. A. Naesseth, F. Lindsten, and T. B. Schön, "High-dimensional filtering using nested sequential monte carlo," *IEEE Trans. Signal Process.*, vol. 67, no. 16, pp. 4177–4188, Jul. 2019.

[50] M. Katzfuss, J. R. Stroud, and C. K. Wikle, "Understanding the ensemble Kalman filter," *Amer. Stat.*, vol. 70, no. 4, pp. 350–357, Oct. 2016.

[51] A. Campbell, Y. Shi, T. Rainforth, and A. Doucet, "Online variational filtering and parameter learning," in *Proc. Adv. Neural Inf. Process. Syst. (NeurIPS)*, Virtual, Online, Dec. 2021, pp. 18 633–18 645.

[52] C. Rosato, L. Devlin, V. Beraud, P. Horridge, T. B. Schön, and S. Maskell, "Efficient learning of the parameters of non-linear models using differentiable resampling in particle filters," *IEEE Trans. Signal Process.*, vol. 70, pp. 3676–3692, Jul. 2022.

[53] Y. Chen, D. Sanz-Alonso, and R. Willett, "Autodifferentiable ensemble Kalman filters," *SIAM J. Math. Data Sci.*, vol. 4, no. 2, pp. 801–833, Jun. 2022.

[54] ——, "Reduced-order autodifferentiable ensemble Kalman filters," *Inverse Probl.*, vol. 39, no. 12, p. 124001, Oct. 2023.

[55] T. Ishizone, T. Higuchi, and K. Nakamura, "Ensemble Kalman variational objective: A variational inference framework for sequential variational auto-encoders," *Nonlinear Theory and Its Applications, IEICE*, vol. 14, no. 4, pp. 691–717, Oct. 2023.

[56] J. Courts, A. G. Wills, T. B. Schön, and B. Ninness, "Variational system identification for nonlinear state-space models," *Automatica*, vol. 147, p. 110687, Jan. 2023.

[57] K. D. Polyzos, Q. Lu, and G. B. Giannakis, "Ensemble Gaussian processes for online learning over graphs with adaptivity and scalability," *IEEE Trans. Signal Process.*, vol. 70, pp. 17–30, Oct. 2021.

[58] Y. Zhao, J. Nassar, I. Jordan, M. Bugallo, and I. M. Park, "Streaming variational Monte Carlo," *IEEE Trans. Pattern Anal. Mach. Intell.*, vol. 45, no. 1, pp. 1150–1161, Feb. 2022.

[59] M. Dowling, Y. Zhao, and I. M. Park, "Real-time variational method for learning neural trajectory and its dynamics," in *Proc. Int. Conf. Learn. Represent. (ICLR)*, 2023.

[60] Y. Zhao and I. M. Park, "Variational online learning of neural dynamics," *Front. Comput. Neurosci.*, vol. 14, p. 71, Oct. 2020.

[61] S. Linderman, M. Johnson, A. Miller, R. Adams, D. Blei, and L. Paninski, "Bayesian learning and inference in recurrent switching linear dynamical systems," in *Proc. Int. Conf. Artif. Intell. Stat. (AISTATS)*, Fort Lauderdale, FL, United states, Apr. 2017, pp. 914–922.

SUPPLEMENT A
VARIATIONAL BAYES

A. Evidence Lower Bound (ELBO)

In Bayesian statistics, the model marginal likelihood $p(\vec{y}|\theta)$ is a fundamental quantity for model selection and comparison [41]. By maximizing the logarithm of $p(\vec{y}|\theta)$ w.r.t. the model parameters θ , the goodness of data fitting and the model complexity are automatically balanced, in accordance with Occam's razor principle [40]. However, $p(\vec{y}|\theta)$ is obtained by integrating out all the latent variables $\{\vec{x}, \vec{f}\}$ in the joint distribution, see Eq. (15), which is analytically intractable. Thus, the posterior distribution of the latent variables, $p(\vec{x}, \vec{f}|\vec{y}) = \frac{p(\vec{y}, \vec{x}, \vec{f})}{p(\vec{y}|\theta)}$, cannot be expressed in a closed-form analytical expression, either. This intractability issue has been addressed in variational Bayesian methods by adopting a variational distribution [2], $q(\vec{x}, \vec{f})$, to approximate the intractable $p(\vec{x}, \vec{f}|\vec{y})$. With the newly introduced variational distribution $q(\vec{x}, \vec{f})$, we have

$$\begin{aligned}
 \log p(\vec{y}|\theta) &= \log \frac{p(\vec{y}, \vec{x}, \vec{f})}{p(\vec{x}, \vec{f}|\vec{y})} \\
 &= \int \int q(\vec{x}, \vec{f}) \log \frac{p(\vec{y}, \vec{x}, \vec{f})q(\vec{x}, \vec{f})}{p(\vec{x}, \vec{f}|\vec{y})q(\vec{x}, \vec{f})} d\vec{x} d\vec{f} \\
 &= \underbrace{\mathbb{E}_{q(\vec{x}, \vec{f})} \left[\log \frac{p(\vec{y}, \vec{x}, \vec{f})}{q(\vec{x}, \vec{f})} \right]}_{\text{ELBO: } \mathcal{L}} + \underbrace{\mathbb{E}_{q(\vec{x}, \vec{f})} \left[\log \frac{q(\vec{x}, \vec{f})}{p(\vec{x}, \vec{f}|\vec{y})} \right]}_{\text{KL divergence}}
 \end{aligned} \tag{39}$$

SUPPLEMENT B
MORE EXPERIMENT RESULTS

A. OEnVI: Online Learning Results on Linear Gaussian SSMs

- The definition of RMSE:

$$\text{RMSE} = \sqrt{\frac{1}{T} \sum_{t=1}^T \sum_{d=1}^{d_x} (\hat{\mathbf{x}}_t^{(d)} - \mathbf{x}_t^{(d)})^2} \tag{40}$$

where $\hat{\mathbf{x}}_t$ represents the estimation of \mathbf{x}_t .

- The baseline in Table III is the RMSE between the noisy observations $\mathbf{y}_{1:T}$ and the latent states $\mathbf{x}_{1:T}$

TABLE III
STATE INFERENCE PERFORMANCE (RMSE) OF ENVI AND OENVI

Time Slot	0 – 120	120 – 240	240 – 360	360–480	480–600	600–720	720–840	840–960	900–1000	0–1000
KF	0.5252	0.5149	0.5228	0.5658	0.5246	0.4907	0.4983	0.5202	0.4846	0.5199
EnVI	0.6841	/	/	/	/	/	/	/	/	0.7182
OEnVI	0.7784	0.7130	0.6512	0.6487	0.6786	0.6515	0.5958	0.6713	0.6418	0.6739
Baseline	0.9872	0.9811	0.9510	1.0077	1.0215	0.9967	1.0077	1.0314	1.0222	0.9974

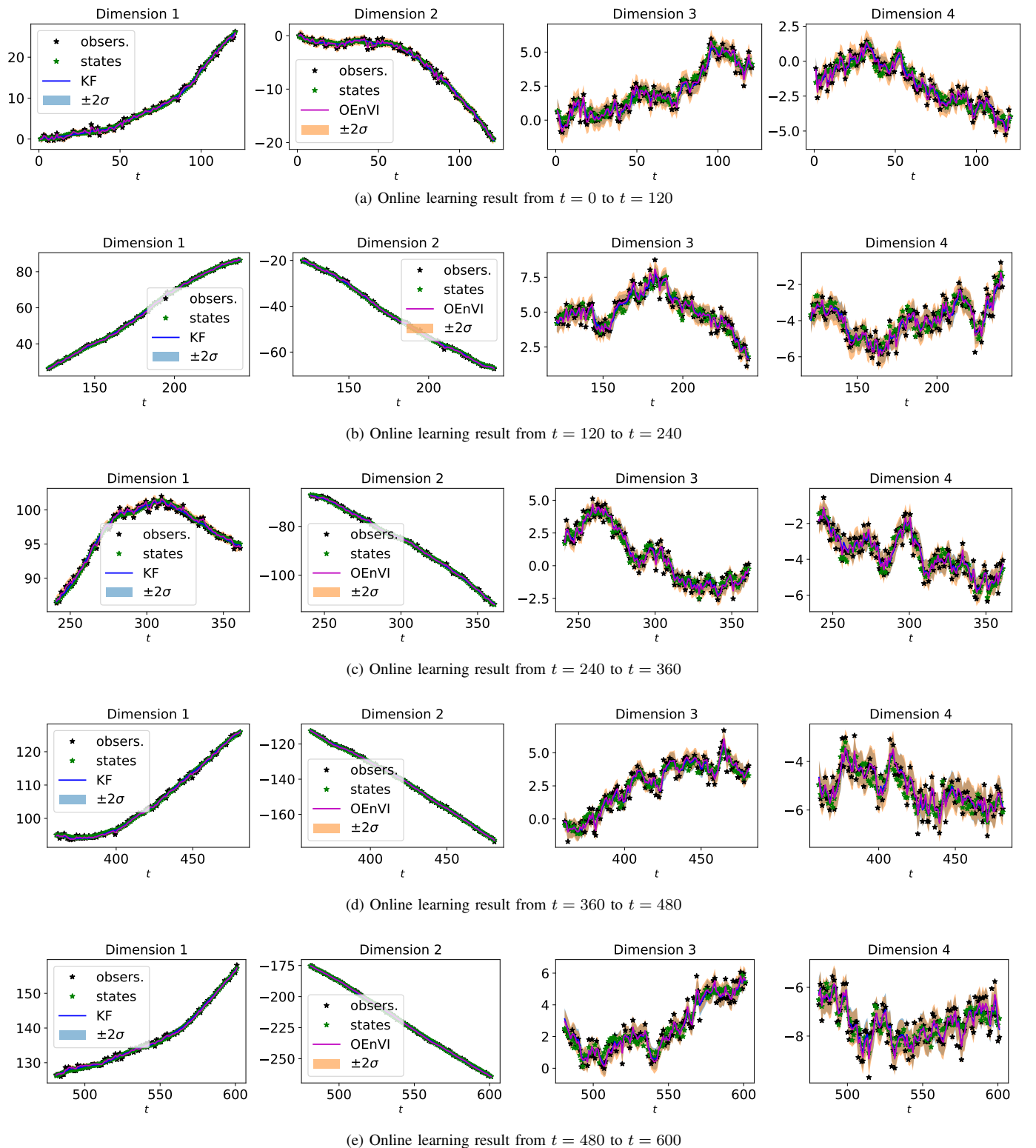


Fig. 6. OEnVI on learning and inference in linear Gaussian SSMs

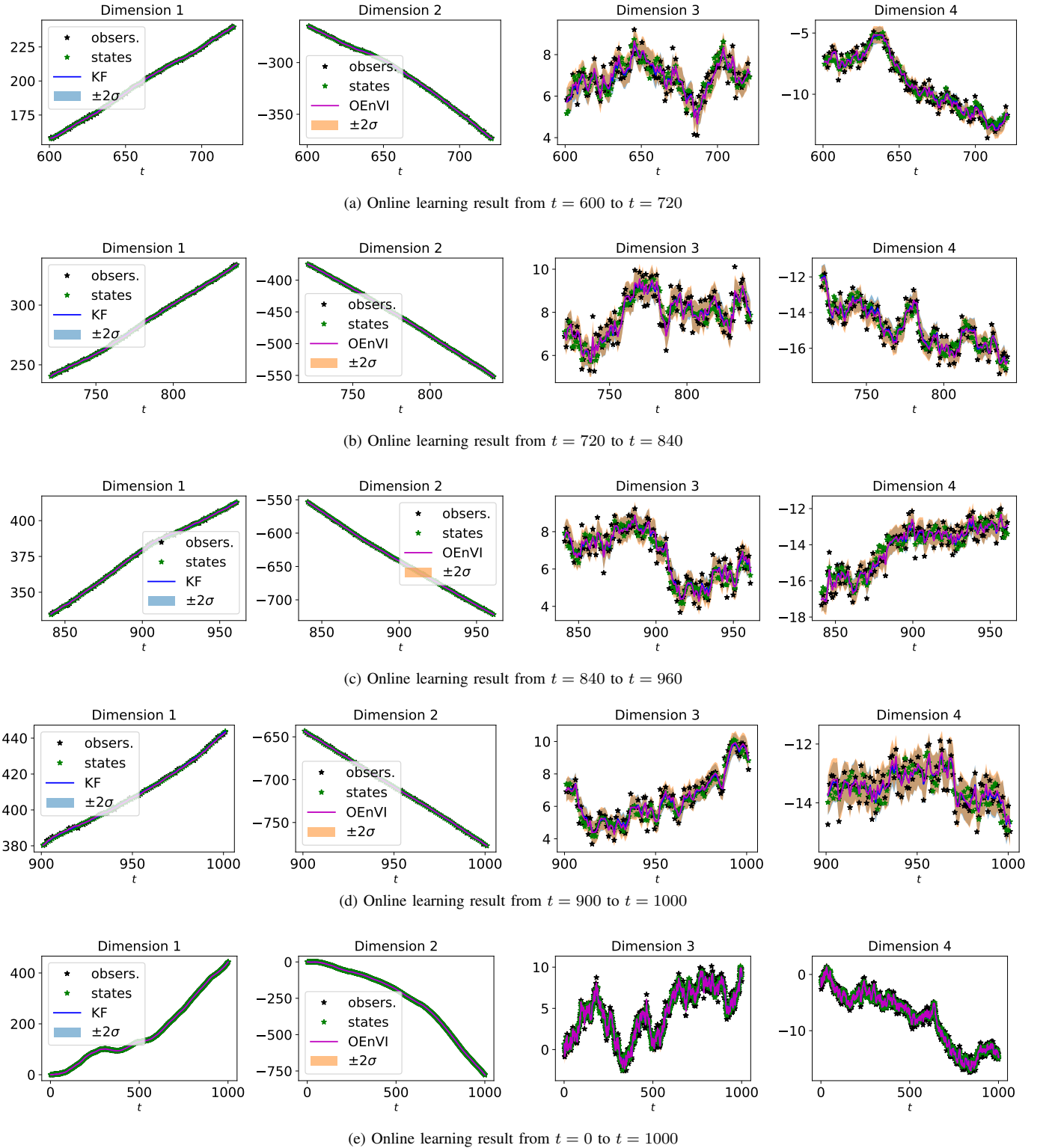


Fig. 7. OEnVI on learning and inference in linear Gaussian SSMs

B. Learning System Dynamics on Kink Function

- The kink function is depicted in Fig. 8
- The MSE and Log-likelihood in Table I are evaluated as follows:

$$\text{MSE} = \frac{1}{T} \sum_{t=1}^T \sum_{d=1}^{d_x} (\hat{\mathbf{f}}_t^{(d)} - \mathbf{f}_t^{(d)})^2 \quad (41)$$

$$\text{Log-likelihood} = \frac{1}{T} \sum_{t=1}^T \log \mathcal{N}(\mathbf{f}_t \mid \xi_t, \Xi_t) \quad (42)$$

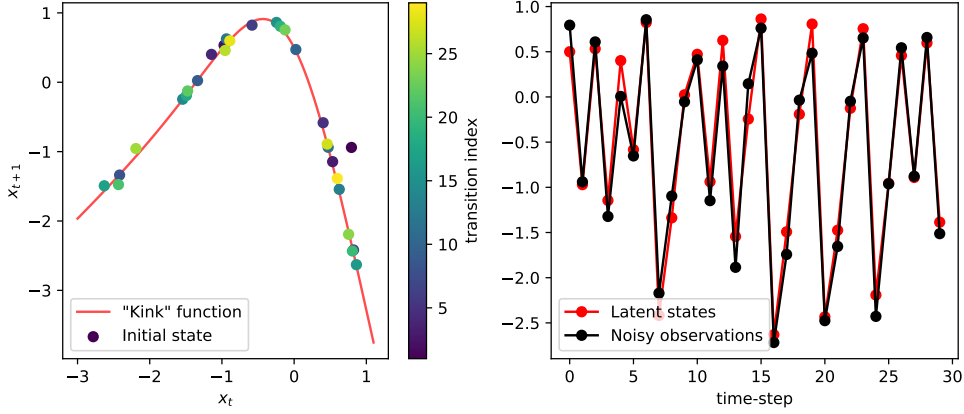


Fig. 8. The "kink" dynamical function is used to generate 50 latent states and corresponding observations, with $\sigma_Q^2 = 0.01$ and $\sigma_R^2 = 0.1$.

C. Time Series Data Forecasting using EnVI

In addition to the overall prediction performance outlined in Table II, we provide a specific prediction of EnVI below.

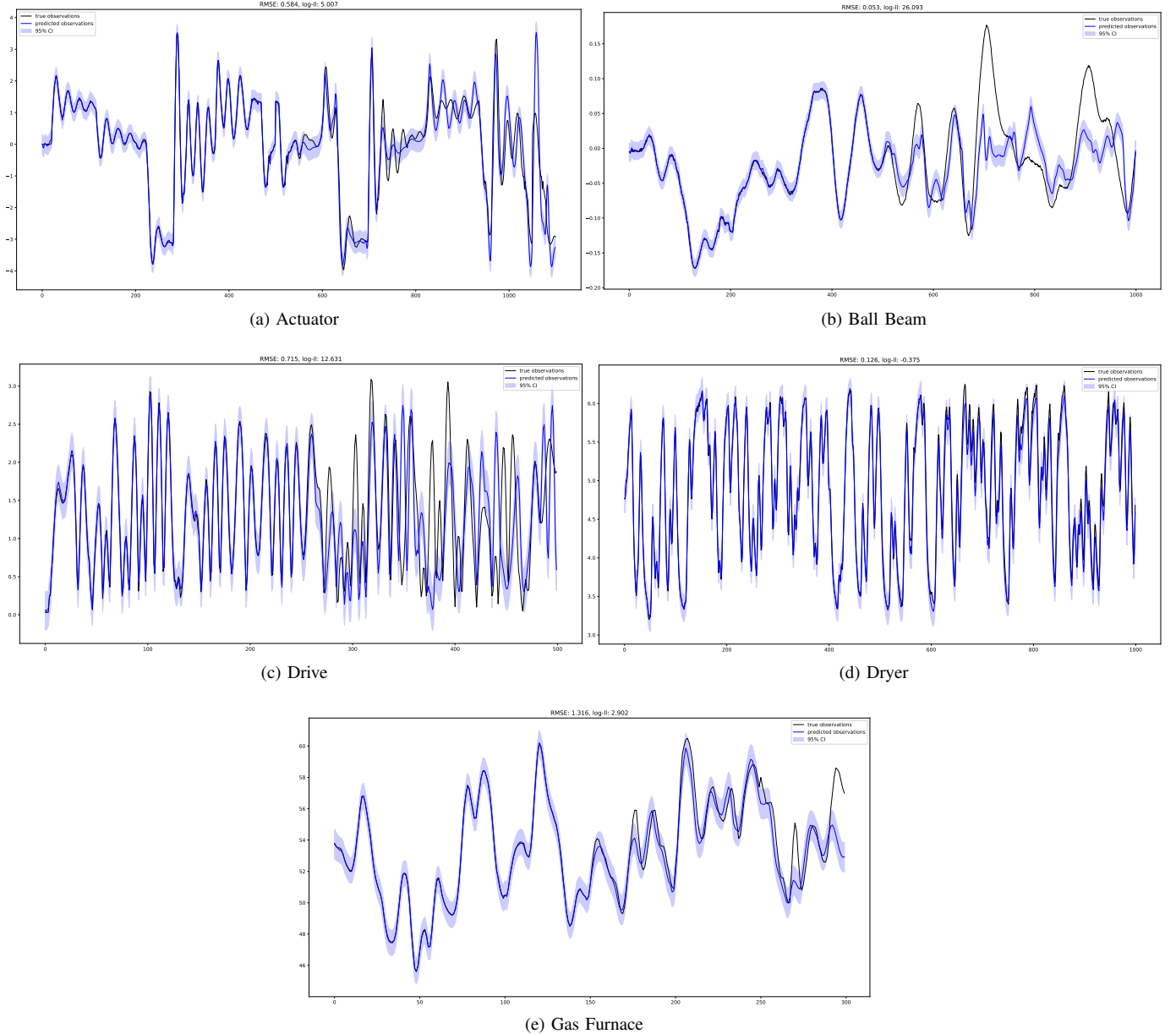


Fig. 9. Learning and prediction results of EnVI. The initial half of the sequence is generated by passing the filtered \mathbf{x}_t through the emission model, while the subsequent half of the sequence represents the prediction outcome. This prediction is derived from the filtered \mathbf{x}_t obtained from the final step of the training sequence, serving as the initial state.

D. Online Learning and Inference with OEnVI

We report the learning results of OEnVI on the kink function dataset. As illustrated in Fig. 10, after sequentially training with 600 data points, OEnVI demonstrates comparable performance to EnVI, which undergoes offline training consisting of over 400 iterations with a full batch of data with length $T=600$.

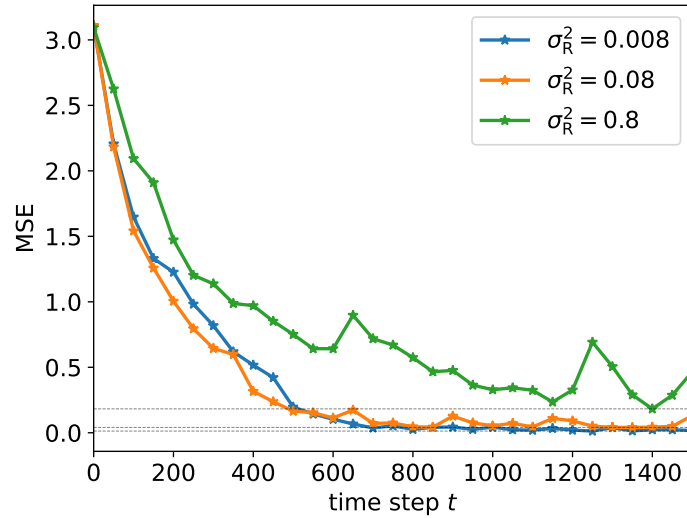


Fig. 10. Kink transition function learning using Online EnVI